Regular Article

blood

HEMATOPOIESIS AND STEM CELLS

Genomic and functional integrity of the hematopoietic system requires tolerance of oxidative DNA lesions

Ana Martín-Pardillos,[1,*] Anastasia Tsaalbi-Shtylik,[1,*] Si Chen,[2] Seka Lazare,[3] Ronald P. van Os,[3] Albertina Dethmers-Ausema,[3] Nima Borhan Fakouri,[4] Matthias Bosshard,[5] Rossana Aprigliano,[5,6] Barbara van Loon,[5,6] Daniela C. F. Salvatori,[7] Keiji Hashimoto,[8] Celia Dingemanse-van der Spek,[1] Masaaki Moriya,[8] Lene Juel Rasmussen,[4] Gerald de Haan,[3] Marc H. G. P. Raaijmakers,[2] and Niels de Wind[1]

[1]Department of Human Genetics, Leiden University Medical Center, Leiden, The Netherlands; [2]Department of Hematology, Erasmus Medical Center Cancer Institute, Rotterdam, The Netherlands; [3]European Research Institute for the Biology of Ageing, University Medical Centre Groningen, University of Groningen, Groningen, The Netherlands; [4]Center for Healthy Aging, Department of Cellular and Molecular Medicine, University of Copenhagen, Copenhagen, Denmark; [5]Department of Molecular Mechanisms of Disease, University of Zürich, Zürich, Switzerland; [6]Department of Cancer Research and Molecular Medicine, Norwegian University for Science and Technology, Trondheim, Norway; [7]Department of Pathology, Leiden University Medical Center, Leiden, The Netherlands; and [8]Department of Pharmacological Sciences, Stony Brook University Medical School, Stony Brook, NY

Key Points

- Tolerance of oxidative DNA lesions ensures the genomic and functional integrity of hematopoietic stem and precursor cells.
- Endogenous DNA damage–induced replication stress is associated with mitochondrial dysfunction.

Endogenous DNA damage is causally associated with the functional decline and transformation of stem cells that characterize aging. DNA lesions that have escaped DNA repair can induce replication stress and genomic breaks that induce senescence and apoptosis. It is not clear how stem and proliferating cells cope with accumulating endogenous DNA lesions and how these ultimately affect the physiology of cells and tissues. Here we have addressed these questions by investigating the hematopoietic system of mice deficient for *Rev1*, a core factor in DNA translesion synthesis (TLS), the postreplicative bypass of damaged nucleotides. *Rev1* hematopoietic stem and progenitor cells displayed compromised proliferation, and replication stress that could be rescued with an antioxidant. The additional disruption of *Xpc*, essential for global-genome nucleotide excision repair (ggNER) of helix-distorting nucleotide lesions, resulted in the perinatal loss of hematopoietic stem cells, progressive loss of bone marrow, and fatal aplastic anemia between 3 and 4 months of age. This was associated with replication stress, genomic breaks, DNA damage signaling, senescence, and apoptosis in bone marrow. Surprisingly, the collapse of the *Rev1Xpc* bone marrow was associated with progressive mitochondrial dysfunction and consequent exacerbation of oxidative stress. These data reveal that, to protect its genomic and functional integrity, the hematopoietic system critically depends on the combined activities of repair and replication of helix-distorting oxidative nucleotide lesions by ggNER and Rev1-dependent TLS, respectively. The error-prone nature of TLS may provide mechanistic understanding of the accumulation of mutations in the hematopoietic system upon aging. (*Blood*. 2017;130(13):1523-1534)

Introduction

The aging-associated attrition of proliferating tissues is accompanied by mutagenesis and genomic rearrangements, cellular senescence, and mitochondrial dysfunction, possibly in response to the accumulation of endogenous DNA damage.[1] Each cell in the body acquires 10^4 to 10^5 endogenous DNA lesions per day.[2] Most DNA lesions are repaired by a network of complementary DNA repair systems, each of which deals with a specific class of lesions, as an integral part of the DNA damage response (reviewed in Mandal et al,[3] Blanpain et al,[4] and Vitale et al[5]). The dominant, global-genome, nucleotide excision repair (ggNER; Figure 1A) pathway specifically recognizes and removes helix-distorting endogenous and exogenous nucleotide lesions.[6] ggNER deficiency, as exemplified by mice with a disruption of the *Xpc* gene, only causes minor phenotypes when the organism is not exposed to exogenous genotoxic agents. This result suggests that unrepaired endogenous helix-distorting DNA lesions can be tolerated at the genome of proliferating cells.[6,7] Unrepaired nucleotide lesions usually arrest processive replication forks, resulting in lesion-containing single-stranded DNA (ssDNA) tracts. Persistent ssDNA tracts can collapse to cytotoxic and recombinogenic dsDNA breaks. To fill such lesion-containing ssDNA tracts and to enable termination of genomic replication, cells have evolved multiple mechanisms, collectively called DNA damage tolerance.[8] Thereby, these mechanisms prevent genomic instability, senescence, and apoptosis caused by unreplicated damaged nucleotides. DNA translesion synthesis (TLS) is the major DNA damage tolerance mechanism

Submitted 25 January 2017; accepted 10 August 2017. Prepublished online as *Blood* First Edition paper, 21 August 2017; DOI 10.1182/blood-2017-01-764274.

*A.M.-P. and A.T.-S. contributed equally to this study.

The online version of this article contains a data supplement.

The publication costs of this article were defrayed in part by page charge payment. Therefore, and solely to indicate this fact, this article is hereby marked "advertisement" in accordance with 18 USC section 1734.

in mammals. TLS employs specialized DNA polymerases to directly replicate across damaged nucleotides. Because these TLS polymerases frequently misincorporate opposite the lesion, cellular survival by TLS comes at the expense of nucleotide substitution mutagenesis (Figure 1A).[9] The core TLS polymerase Rev1 inserts cytidines opposite abasic nucleotides and a limited spectrum of nucleotide adducts at the minor groove of the DNA helix.[10,11] Additionally, Rev1 plays an important regulatory role in TLS of helix-distorting nucleotide lesions, of (nondamaged) G-quadruplex structures,[12] whereas it also operates in the repair of interstrand DNA cross-links.[9,13]

The long-lived nature of hematopoietic stem cells (HSCs) makes these cells particularly susceptible to endogenous and exogenous genotoxic insults that can limit their functional capacity and that also induce genomic alterations that predispose to hematopoietic malignancies.[14] Therefore, the hematopoietic system provides a paradigm to study the involvement of endogenous DNA damage in development, maintenance, decay, and cancer development of proliferating and differentiating tissues.[14-18]

Here we investigated the role of Rev1-dependent TLS in the development and maintenance of the hematopoietic system. We reveal the requirement of TLS opposite unrepaired endogenous helix-distorting DNA lesions for the maintenance of hematopoietic stem and precursor cells (HSPCs). We furthermore demonstrate that ggNER and, to a greater extent, TLS provide independent and complementary mechanisms to protect the hematopoietic system against the detrimental phenotypes caused by endogenous DNA lesions.

Methods in brief

Full methods are included in the supplemental Data (available on the *Blood* Web site).

Mice and cell lines

All mouse experiments were approved by the ethical review board of the Institute, and the specific pathogen-free mice were kept according to Federation of Laboratory Animal Science Associations guidelines. Wild-type (WT), *Rev1*,[19] *Xpc*, and *Rev1Xpc* mouse cohorts were obtained by crossing FVB and C57Bl/6 parents. Equal numbers of hybrid males and females were used for most experiments. Transplantation experiments using *Rev1* animals were performed in the C57Bl/6 background. Hairless albino SKH-1 mice were used for measuring sensitivity of the skin to UV light–induced nucleotide lesions.

Competitive transplantation experiments using Rev1 hematopoietic cells were performed as follows: whole bone marrow or isolated HSCs (alone or, when indicated, together with W41.SJL [c-kit receptor-mutant bone marrow cells]) from donors were introduced into lethally irradiated B6.SJL recipients. Secondary transplantation was performed as previously described.[20] Chimerism of the hematopoietic system was analyzed at different time points after transplantation using multiplex polymerase chain reaction (PCR) on blood. Reconstitution of the *Rev1Xpc* bone marrow with *Xpc* bone marrow was performed at the age of 1.5 months, by injecting 5×10^6 *Xpc* bone marrow cells. Unless stated otherwise, mice were given an intraperitoneal injection with 5-bromo-2′-deoxyuridine (BrdU) and ethynyl-2′-deoxyuridine (EdU), 1 hour before euthanization with CO_2, to label replicating cells. Mouse embryonic fibroblast (MEF) lines were obtained by spontaneous immortalization of fibroblasts from 13.5-day embryos of the hybrid background. Survival after genotoxin exposure was measured using clonogenic assays.

Whole blood analysis

For whole blood analysis, peripheral blood was manually or automatically counted. For the quantification of white blood cell ratios and Howell-Jolly bodies, blood smears were stained with Giemsa.

Bone marrow and blood preparation for stainings

Bone marrow cells were extracted by flushing femurs and tibia. One intact femur was used to calculate bone marrow cellularities. Cell numbers were normalized to body weight. Paraffin-embedded sections were stained with hematoxylin and eosin. Whole blood was extracted from heart. Erythrocytes were lysed before characterization of hematopoietic and blood cells.

Analysis of cultured HSCs

Long-term-HSCs were isolated and cultured for 2 weeks with or without 100 μM *N*-acetylcysteine (NAC). Colony sizes were scored at day 7 and day 14. At day 14, cells were collected for immunofluorescence staining of the DNA damage marker γH2AX.

Cobblestone area–forming cell (CAFC) assay

The CAFC assay assesses the clonogenicity and size in vitro of different HSPC populations and was performed as previously described.[21,22]

Analysis of HSPC populations

HSPC populations were isolated by fluorescence-activated cell sorting, following labeling of HSPC population-specific surface markers with antibodies and labeling these with fluorophores. Concentrations and origin of these reagents are depicted in supplemental Table 1. To identify stromal cells, bone marrow cell suspensions were stained with the stromal cell–specific antibodies followed with fluorophore labeling and fluorescence-activated cell sorting. Fetal livers were analyzed after BrdU injection of the mother. Fetal liver cell suspensions were stained with cell surface markers for HSPCs (supplemental Table 1), followed by BrdU staining. For the analysis of proliferation and apoptosis, freshly isolated fetal liver cells were stained with HSPC cell surface markers and then for Ki67 or annexin V, respectively. 7-Amino-actinomycin D was added in the cell suspension to stain DNA prior to analysis to exclude dead cells. Data were acquired using flow cytometry.

Immunohistochemistry and immunofluorescence

Whole bone marrow cells were fixated on cytospin adhesion slides and stained for BrdU, caspase-3, Dec1,[23] γ-H2AX, Ki67, p16, 8-hydroxy-2′-deoxyguanosine (8OHdG), phospho-p38, or 53BP1. Staining for incorporated EdU was performed according to the manufacturers' instructions. Staining of bone marrow for 4-hydroxynonenal (4-HNE) was performed on deparaffinized sections after antigen retrieval. Sections were counterstained with Mayers hemalum.

Alkaline comet assays

Alkaline single-cell electrophoresis ("comet") assays that enable us to detect ssDNA and dsDNA breaks at the genome, and staining for incorporated BrdU to identify S-phase nuclei, were performed on bone marrow cell suspensions, essentially as described.[24]

TLS assay

The generation of a site-specific single-stranded H-εdC lesion and the determination of the efficiency and mutagenicity of TLS

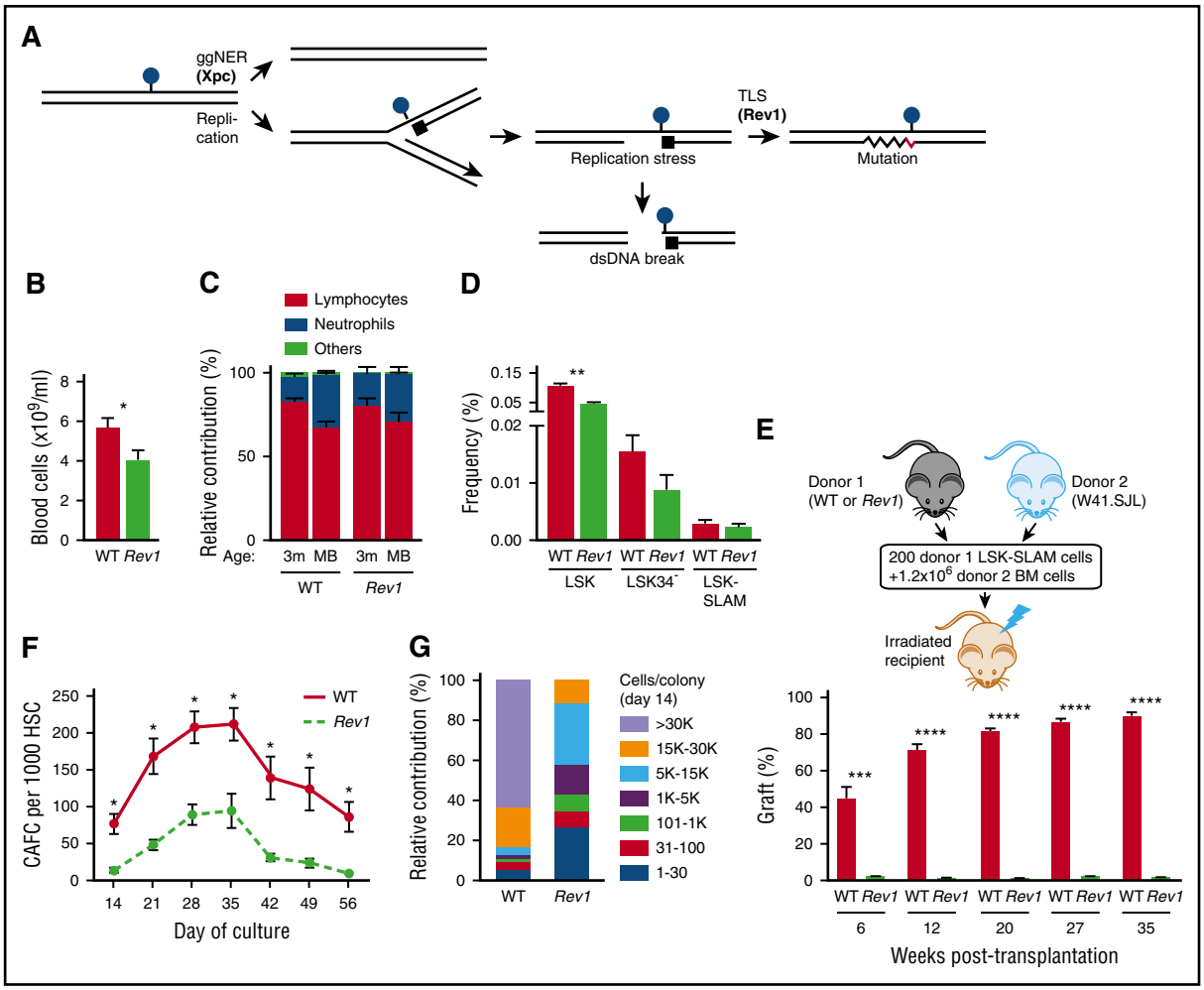

Figure 1. *Rev1* hematopoietic stem cell (HSC) display competitive and proliferative defects (see also supplemental Figure 1). The involvement of TLS in tolerance of endogenous DNA damage in the hematopoietic system was investigated by analyzing *Rev1* blood and bone marrow, by competitive repopulation experiments, and by culture of hematopoietic stem and progenitor cells (HSPCs) in vitro. $^{*}P < .05$; $^{**}P < .01$; $^{***}P < .001$; $^{****}P < .0001$. Data are mean ± standard error of the mean (SEM). (A) Helix-distorting nucleotide lesions (blue spheres) can be repaired by ggNER, dependent on the *Xpc* gene. In case a lesion escapes timely repair, it arrests processive replication (black rectangle), resulting in replication stress and DNA damage signaling. The lesion can be bypassed postreplicatively by *Rev1*-dependent DNA TLS (zig-zag line). Thereby, TLS prevents the induction of replication stress and double-stranded DNA (dsDNA) breaks. TLS frequently misincorporates (in red) opposite the damaged nucleotide, which originates nucleotide substitution mutations. (B) Cytopenia in 26- to 30-month-old *Rev1* mice (n = 11), compared with age-matched WT mice (n = 6). (C) Relative contribution of myeloid and lymphoid cells in the WT and *Rev1* blood at 3 months of age (3m) and when moribund (MB). N = 10. (D) Frequencies of LSK, LSK34-, and LSK-SLAM cells in bone marrow of 5-month-old *Rev1* (n = 5) and WT mice (n = 5). Frequencies are depicted as percent of mononuclear cells. (E) Impaired function of *Rev1*-deficient HSCs as demonstrated by competitive repopulation assays. Scheme of competitive transplantation experiments (top). Competitive transplantation of WT (n = 9) and *Rev1* HSCs (n = 8) (bottom). (See also supplemental Figure 1.) (F) Impaired proliferative capacity of HSPCs as demonstrated by reduced CAFC numbers from 5-month-old WT (n = 4) and *Rev1* (n = 4) mice. (G) Sizes of colonies after single-cell sorting of LSK-SLAM cells from 5-month-old *Rev1* (n = 3) and WT (n = 3) mice.

were performed essentially as described for a benzo[a]pyrene-dG adduct.[25]

Analysis of mitochondrial function

Mitochondrial membrane potentials were measured by flow cytometry. Measurement of mitochondrial DNA (mtDNA) was performed by quantitative PCR. The relative mtDNA levels were calculated using equation $2 \times 2^{\Delta CT}$. Mitochondrial respiration of freshly isolated total bone marrow cells was analyzed using a Seahorse extracellular flux bioanalyzer. For western blotting of mitochondrial proteins, freshly frozen bone marrow cells were resuspended in radioimmunoprecipitation assay buffer followed by brief sonication. Electrophoresis, blotting, antibody incubations, and visualization of signals using enhanced chemiluminescence were performed using standard protocols.

Results

Rev1 contributes to HSPC maintenance

Rev1-deficient mice displayed mild cytopenia of the blood, affecting all lineages (Figure 1B-C). Analysis of short- and long-term HSC populations revealed a slight, but significant, decrease in the frequency of early hematopoietic progenitors (LSK cells), already at a young age (Figure 1D). Competitive repopulation experiments revealed that long-term *Rev1* HSCs (the LSK-SLAM population) were unable to compete with simultaneously administered W41.SJL HSCs[20] (which themselves display compromised repopulation capacity) in reconstituting the bone marrow of lethally irradiated WT mice (Figure 1E). Even in the absence of W41.SJL competitors, *Rev1* HSCs repopulated the recipients'

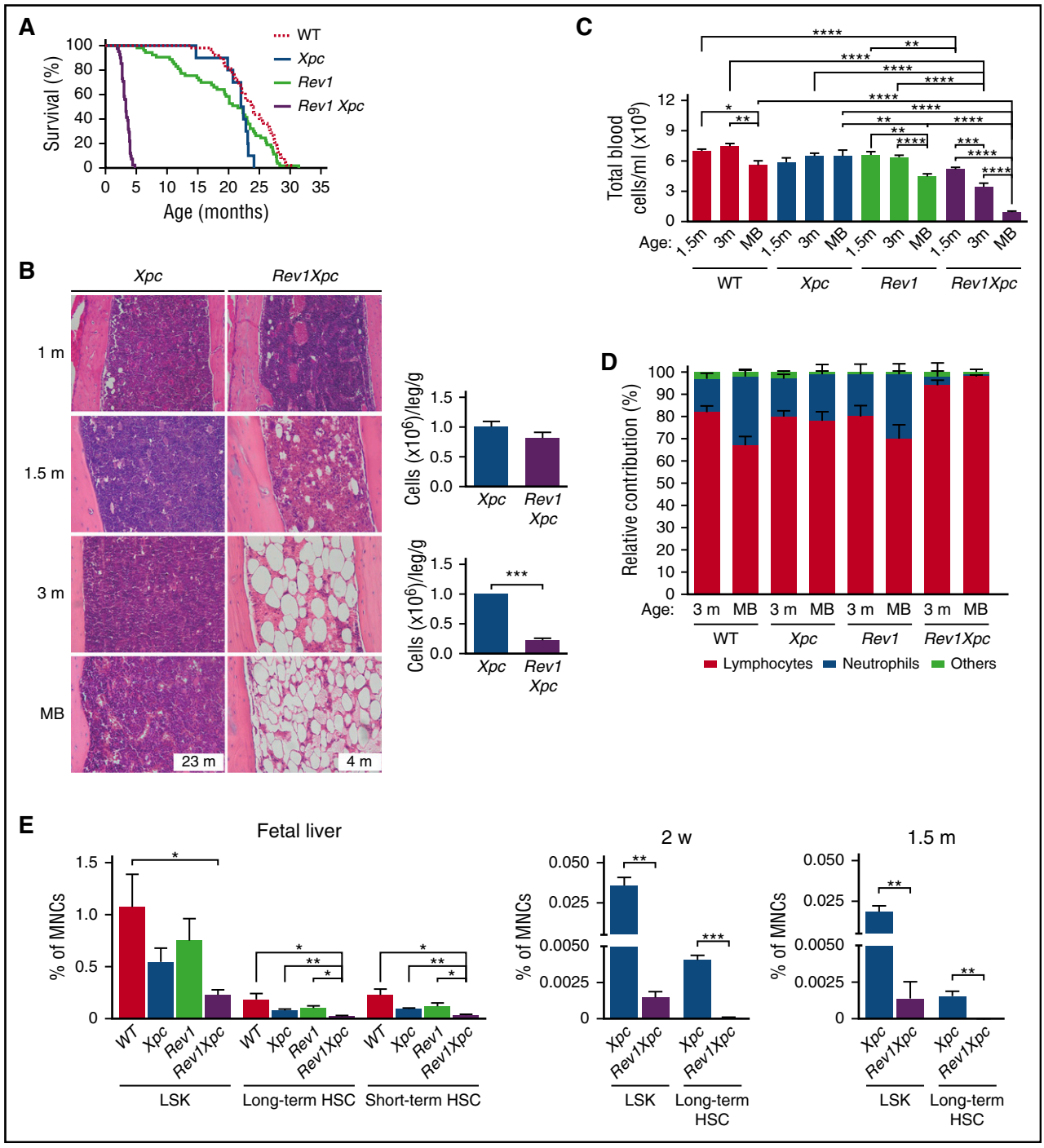

Figure 2. Rev1-dependent tolerance of unrepaired endogenous nucleotide lesions protects HSCs (see also supplemental Figures 2 and 3). Analysis of the hematopoietic system of WT, ggNER (*Xpc*), TLS (*Rev1*), and TLS + ggNER (*Rev1Xpc*) mice reveals that ggNER and TLS jointly protect HSPCs against cell-autonomous genotoxicity of endogenous helix-distorting DNA lesions. **P* < .05; ***P* < .01; ****P* < .001; *****P* < .0001. Data are mean ± SEM. (A) Kaplan-Meier curves depicting survival of mice of all 4 genotypes: WT (n = 64), *Xpc* (n = 10), *Rev1* (n = 53), and *Rev1Xpc* (n = 41). Survival of the different genotypes was compared with WT mice using the Wilcoxon test. (B) Progressive bone marrow aplasia in *Rev1Xpc* mice. Bar represents 50 μm. *Xpc*: 1 m (n = 3), 1.5 m (n = 3), 3 m (n = 3), MB (n = 6). *Rev1Xpc*: 1 m (n = 3), 1.5 m (n = 3), 3 m (n = 3), MB (n = 3). Right panels: Quantification of bone marrow cells at 1 (*Xpc*, n = 10; *Rev1Xpc*, n = 11) and 1.5 months (*Xpc*, n = 4; *Rev1Xpc*, n = 4) of age, respectively. (C) *Rev1Xpc* mice develop severe cytopenia. m, months; MB, moribund (see panel A for survival data). WT: 1.5 m (n = 8), 3 m (n = 7), MB (n = 12). *Xpc*: 1.5 m (n = 5), 3 m (n = 12), MB (n = 7). *Rev1*: 1.5 m (n = 6), 3 m (n = 17), MB (n = 33). *Rev1Xpc*: 1.5 m, (n = 10), 3 m (n = 11), MB (n = 10). (D) Relative contribution of myeloid and lymphoid cells in the blood of all genotypes. Note the low contribution of neutrophils specifically in *Rev1Xpc* blood. (E) Bone marrow aplasia in *Rev1Xpc* mice is caused by progressive loss of long-term HSCs (LSK-SLAM cells). MNCs, mononuclear cells. Number of mice analyzed: fetal liver: n = 4 for all genotypes. Two-weeks old: *Xpc* (n = 3), *Rev1Xpc* (n = 3); 1.5-months old: *Xpc* (n = 4), *Rev1Xpc* (n = 4). (F) Increased S/G2/M fractions in *Rev1Xpc* LSK cells, long-term and short term HSCs from fetal liver, suggesting increased replication, as shown by Ki67 staining (G0 cells are Ki67-negative). N = 4 for all genotypes. (G) Increased proliferation of *Rev1Xpc* HSPCs as demonstrated by in vivo BrdU labeling. *Xpc* (n = 3) and *Rev1Xpc* (n = 3) mice. (H) Rescue of early death, bone marrow aplasia, and cytopenia of *Rev1Xpc* mice by transplantation with *Xpc* bone marrow, indicating a hematopoietic cell-intrinsic origin of HSC exhaustion. Survival: *Rev1Xpc* (n = 41), transplanted *Rev1Xpc* (n = 10). Bone marrow: *Rev1Xpc* (n = 3), transplanted *Rev1Xpc* (n = 5). Blood cellularity: *Rev1Xpc* (n = 10), transplanted *Rev1Xpc* (n = 7). Survival of *Rev1Xpc* mice was compared with WT mice using the Wilcoxon test.

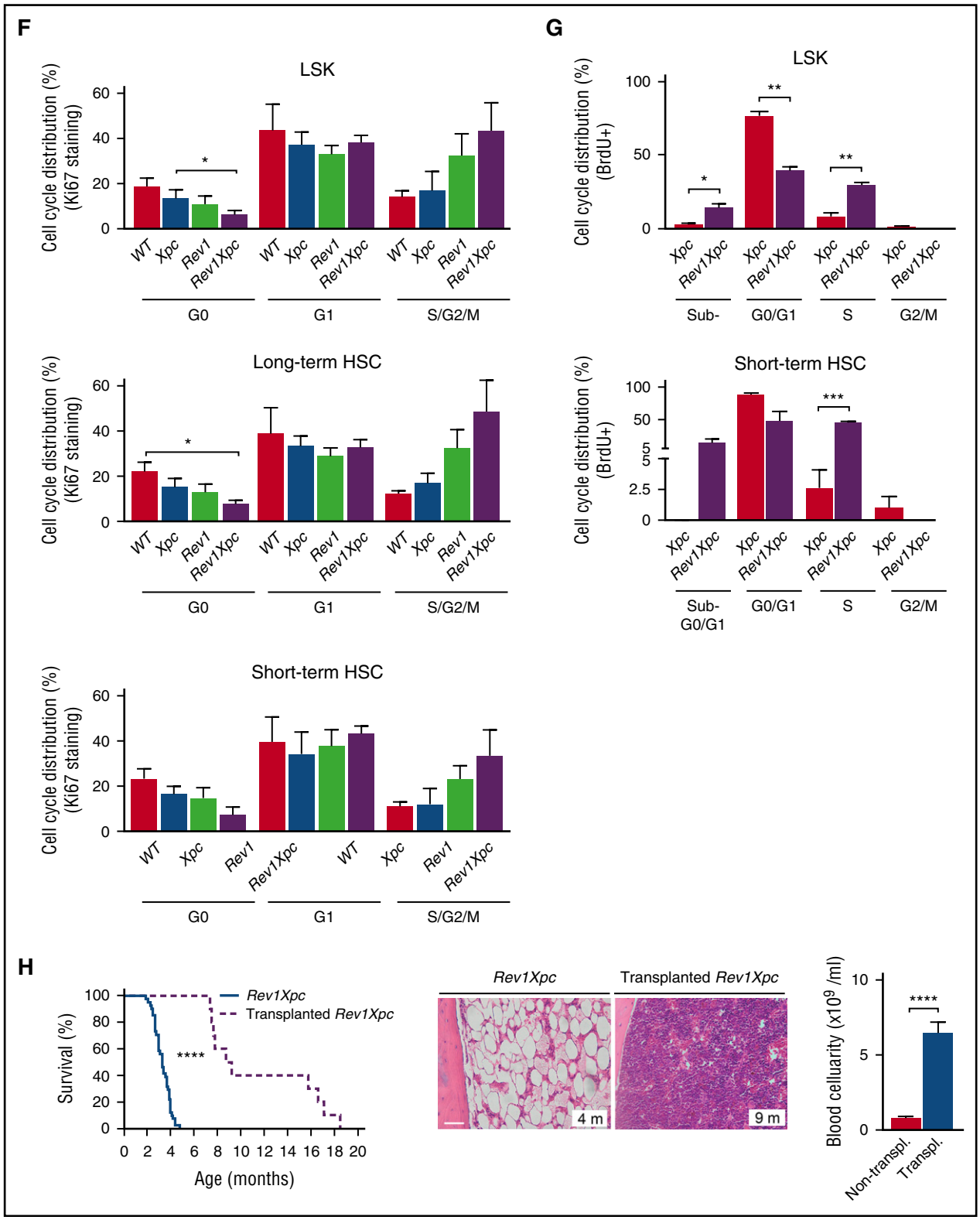

Figure 2. (Continued).

hematopoietic system only inefficiently (supplemental Figure 1A). This phenotype was further aggravated in serial transplantations, indicating a persistent disadvantage of *Rev1* HSCs (supplemental Figure 1B). HSCs isolated from 14-day-old fetal livers already displayed reduced repopulation capacity (supplemental Figure 1C), demonstrating that the attenuation of HSC function occurs early in development and independently of the bone marrow environment. The in vitro clonogenicity of *Rev1*

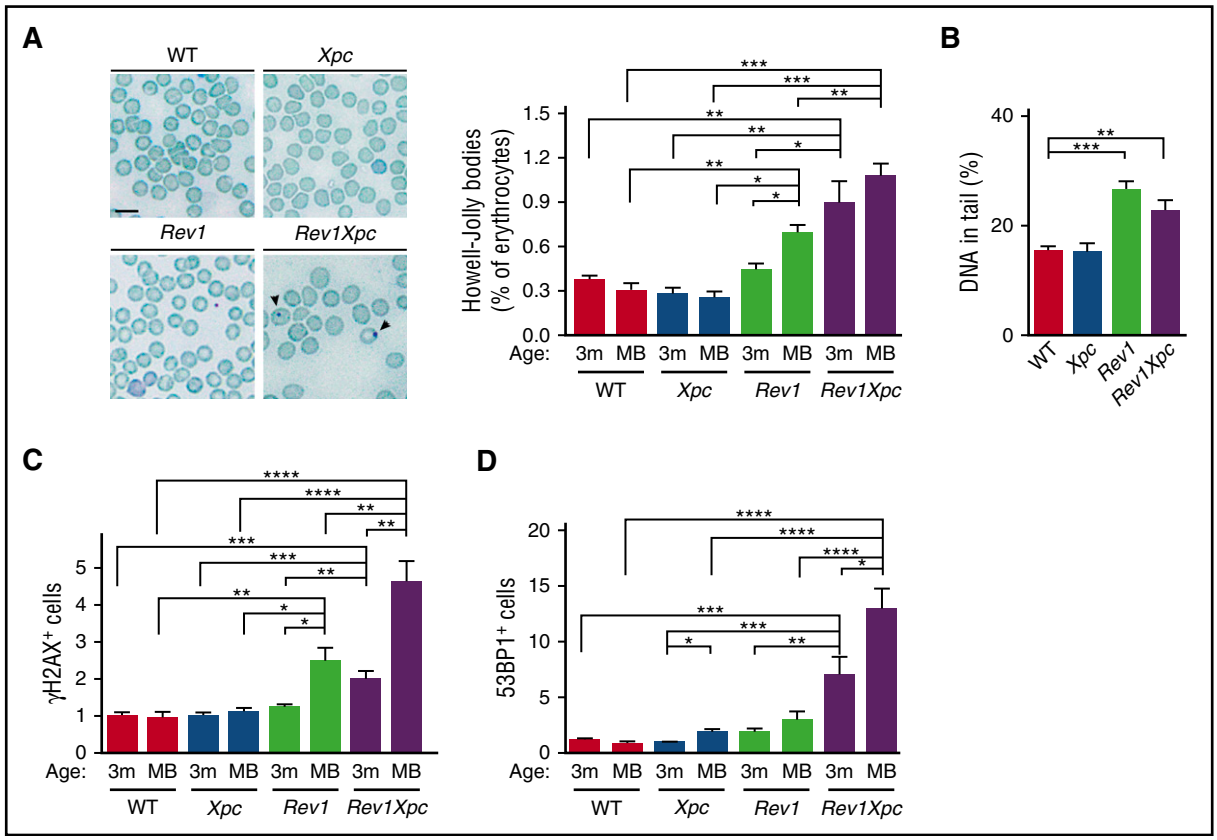

Figure 3. Rev1 protects against replication stress and genomic breaks in the hematopoietic system (see also supplemental Figure 4). We investigated the induction of DNA breaks in the absence of Rev1-mediated TLS at endogenous helix-distorting DNA lesions in blood and bone marrow. *$P < .05$; **$P < .01$; ***$P < .001$; ****$P < .0001$. Data are mean ± SEM. (A) Chromosome fragments (Howell-Jolly bodies, arrowheads) in erythrocytes of 3-month-old *Rev1* and *Rev1Xpc* mice. Bar represents 10 μm. Right panel: quantification. WT: 3 m (n = 5), MB (n = 6). *Xpc*: 3 m (n = 5), MB (n = 6). *Rev1*: 3 m (n = 5), MB (n = 9). *Rev1Xpc*: 3 m (n = 6), MB (n = 8). (B) Chromosome breaks outside of S phase, measured by single-cell alkaline comet gel electrophoresis of bone marrow of 3-month-old mice. WT (n = 4), *Xpc* (n = 4), *Rev1* (n = 4), *Rev1Xpc* (n = 4). Comet intensities of BrdU-negative cells are shown. Increased DNA breaks in bone marrow hematopoietic cells of *Rev1* and *Rev1Xpc* mice as demonstrated by γH2AX (C) and 53BP1 (D) immunostaining. The fraction of positive cells shown was normalized relative to 3-month-old WT. WT: 3 m (n = 8), MB (n = 6). *Xpc*: 3 m (n = 7), MB (n = 6). *Rev1*: 3 m (n = 6), MB (n = 6). *Rev1Xpc*: 3 m (n = 5-6), MB (n = 9).

HSPCs was significantly reduced, compared with WT (Figure 1F), and *Rev1* HSC clones were smaller than controls (Figure 1G). The combined defects in transplantability and in in vitro growth strongly suggest that *Rev1*-deficient HSPCs display compromised proliferative capacity, which most likely is cell intrinsic.

ggNER and TLS synergize to protect the hematopoietic system from the genotoxicity of helix-distorting DNA lesions

We argued that, in case the proliferative defects of *Rev1* HSPCs reflect perturbed TLS of endogenous helix-distorting nucleotide lesions, inactivation of ggNER of this class of nucleotide lesions would exacerbate the hematopoietic phenotypes (Figure 1A). Indeed, disruption of *Xpc* synergistically increased the sensitivity of both *Rev1*-deficient skin and MEFs to helix-distorting photolesions induced by UV light[6] (supplemental Figure 2A-B). Previously, we have shown that, upon UV exposure, *Rev1Xpc* MEFs display high levels of replication stress, caused by replicons arrested at unrepaired helix-distorting photolesions.[26] Thus, ggNER and Rev1-dependent TLS jointly protect cells from the genotoxic effects of UV light, by repairing or tolerating photolesions, respectively (see Figure 1A). *Rev1Xpc* embryos were significantly smaller than WT or single-deficient littermates, and the double-deficient mice were born at sub-Mendelian ratios (supplemental Figure 2C-D), consistent with enhanced sensitivity to endogenous helix-distorting nucleotide lesions. Although *Xpc* mice displayed near-WT life spans, *Rev1* single-deficient mice died slightly earlier than their WT littermates (20 vs 23 months of age, on the average; Figure 2A) of various causes unrelated to the hematopoietic defects. This shortened life span suggests that ggNER is not sufficient to repair all of its substrates, making proliferating cells dependent on Rev1-mediated TLS. In contrast, TLS + ggNER double-deficient, *Rev1Xpc* mice died at, on the average, 3.5 months of age (Figure 2A), displaying aplasia of the bone marrow and pancytopenia of bone marrow and blood that most markedly affected neutrophils (Figure 2B-D; supplemental Table 2 and supplemental Figure 2E-H). HSC counts were strongly reduced already in the liver of *Rev1Xpc* fetuses, and this reduction aggravated through life (Figure 2E; supplemental Figure 2I). In conclusion, the hematopoietic phenotypes of *Rev1*-deficient mice are exacerbated synergistically by concomitant ggNER deficiency, which provides a strong argument that failure to replicate endogenous helix-distorting nucleotide lesions results in hematopoietic attrition. We then investigated the fate of *Rev1Xpc* embryonic liver HSCs. All *Rev1Xpc* HSC subpopulations, and also long-term progenitor cells, were characterized by a reduced G0 and increased Ki67-positive S/G2/M fraction, suggesting exit from quiescence and enhanced proliferation or delay in progression through S phase (Figure 2F; supplemental Figure 2J). In support with the latter, the

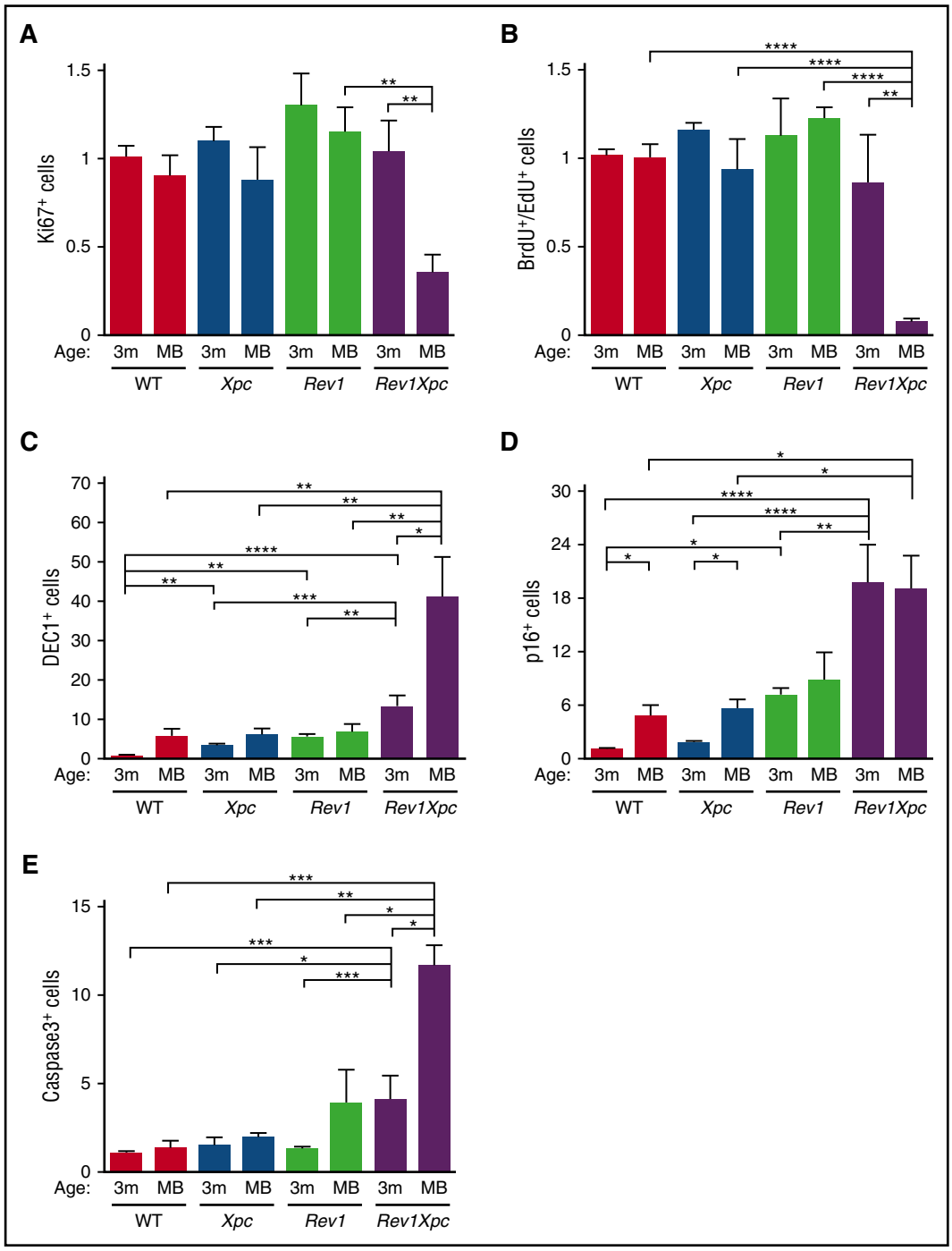

Figure 4. Rev1 protects against endogenous DNA damage–induced senescence and apoptosis (see also supplemental Figure 5). Proliferation, replication, senescence, and apoptosis were quantified in bone marrow of all 4 genotypes. *$P < .05$; **$P < .01$; ***$P < .001$; ****$P < .0001$. Data are mean ± SEM. Reduced proliferation (Ki67 immunostaining) (A) and replication (BrdU and EdU incorporation) (B) in the bone marrow of moribund *Rev1Xpc* mice. WT: 3 m (n = 7-9), MB (n = 5-6). *Xpc*: 3 m (n = 6-8), MB (n = 6). *Rev1*: 3 m (n = 7), MB (n = 6). *Rev1Xpc*: 3 m (n = 6), MB (n = 9). Increased senescence and apoptosis in the bone marrow of *Rev1Xpc* mice as demonstrated by immunostaining for Dec1 (C), p16 (D), and caspase-3 (E). WT: 3 m (n = 4-8), MB (n = 5-6). *Xpc*: 3 m (n = 5-8), MB (n = 5-6). *Rev1*: 3 m (n = 3-7), MB (n = 6). *Rev1Xpc*: 3 m (n = 3-6), MB (n = 6-8). m, months; MB, moribund (see Figure 2A for survival data). The fraction of positive cells shown was normalized relative to 3-month-old WT bone marrow.

fraction of *Rev1Xpc* LSK cells and short-term HSCs that resided in S phase was increased in *Rev1Xpc* embryonic liver HSCs (Figure 2G; supplemental Figure 2K). The concurrent emergence of a BrdU-positive sub-G0 LKS fraction suggested increased death of proliferating *Rev1Xpc* HSCs (Figure 2G; supplemental Figure 2K), although we could not detect increased apoptosis (supplemental Figure 2L).

To confirm aplastic anemia as the cause of death of *Rev1Xpc* mice, we transplanted them with *Xpc* bone marrow cells. This procedure indeed significantly rescued the degenerative hematopoietic phenotypes of these mice and greatly increased their life span (Figure 2H; supplemental Figure 3A). Importantly, these results also suggest that the hematopoietic phenotypes of *Rev1Xpc* mice are cell autonomous. Consistently, the composition of the *Rev1Xpc* bone marrow stromal

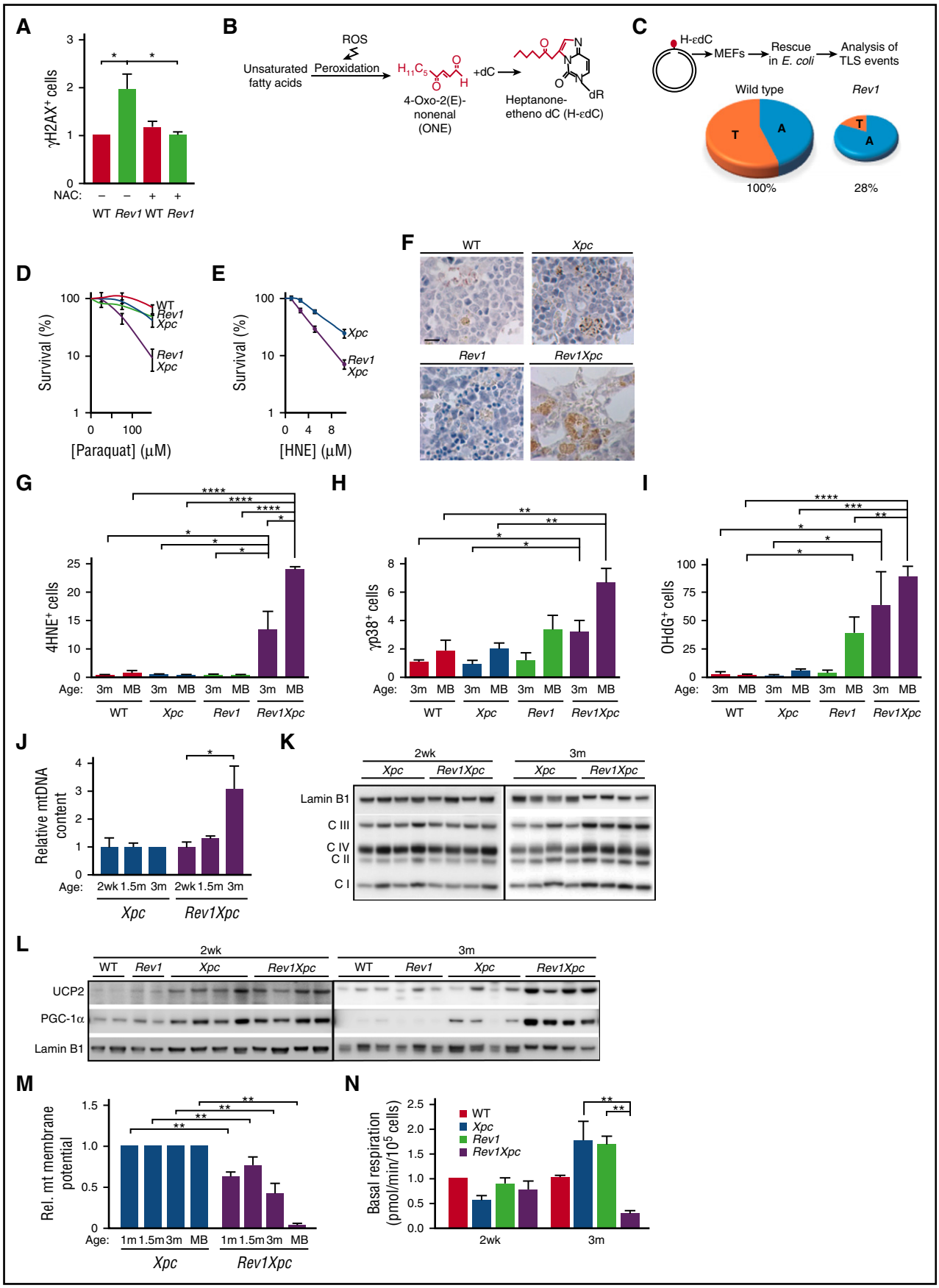

Figure 5.

compartment appeared to be affected only marginally (supplemental Figure 3B-C).

Rev1-dependent TLS protects the bone marrow against replication stress, senescence, apoptosis, and DNA breaks

We wanted to investigate whether Rev1-mediated TLS of endogenous nucleotide lesions protects the genome of hematopoietic cells against DNA breaks. Indeed, whereas erythrocytes normally are devoid of nuclear DNA, blood-derived erythrocytes of *Rev1* and *Rev1Xpc* mice frequently contained chromosomal fragments that presumably were derived from chromosomes broken during the preceding erythroblast stage (so-called Howell-Jolly bodies[27]) (Figure 3A). This phenotype was absent from the *Xpc*-reconstituted *Rev1Xpc* bone marrow, confirming that the DNA breakage was cell intrinsic (supplemental Figure 4A). To assess ssDNA and dsDNA breaks also in bone marrow, we used alkaline single-cell electrophoresis ("comet") assays.[24] Compared with WT HSPCs, *Xpc, Rev1*, and *Rev1Xpc* HSPCs displayed increased comet sizes, and thus increased DNA breaks, during S phase, suggesting arrested replicons, or dsDNA breaks, at endogenous helix-distorting nucleotide lesions (supplemental Figure 4B). However, these breaks persisted beyond S phase only in the absence of Rev1 (Figure 3B; supplemental Figure 4C), indicating that the strand discontinuities were protracted because of the persistent inability to complete genomic replication. In agreement, staining for the DNA breaks and replication stress markers γH2AX and 53BP1[28,29] was increased in bone marrow cells, not only of 3-month-old *Rev1Xpc* mice but also of old *Rev1* mice (Figure 3C-D; supplemental Figure 4D-E). Beyond 3 months of age, proliferation and replication in *Rev1Xpc* bone marrow ceased (Figure 4A-B; supplemental Figure 5A-B), concomitant with the induction of senescence and apoptosis (Figures 4C-E; supplemental Figure 5C-E). Collectively, these data indicate that, in the absence of Rev1, endogenous helix-distorting DNA lesions induce replication stress and genomic breaks that compromise proliferation and viability of HSPCs.

Rev1-dependent TLS provides tolerance of endogenous lipid peroxidation–derived nucleotide adducts

Oxidative DNA lesions are abundant in proliferating cells.[15-18] Moreover, the notion that the *Rev1Xpc* phenotypes are cell autonomous, combined with the specific depletion of neutrophils (see Figure 2D) that produce high levels of reactive oxygen species (ROS),[30] hinted at helix-distorting oxidative DNA lesions as possible culprits for the *Rev1* and *Rev1Xpc* HSPC phenotypes. The scarcity of long-term *Rev1Xpc* HSCs precluded their analysis, and therefore, we investigated responses to endogenous oxidative stress in cultured *Rev1* single-deficient HSCs. Consistent with the results described previously, these cells displayed enhanced γH2AX staining indicating replication stress (Figure 5A; supplemental Figure 6A). However, culture in the presence of the ROS scavenger NAC[31] rescued this γH2AX accumulation (Figure 5A; supplemental Figure 6A-B). This important result confirms that the endogenous ROS induce replication stress in HSC, in the absence of *Rev1*-dependent TLS.

Helix-distorting oxidative nucleotide lesions comprise cyclic purines and long-chain hydroxyalkenal (aldehyde) adducts, and these lesions are derived from lipid peroxidation. Notably, these lesions have been associated with human aging,[32,33] and they represent endogenous substrates for ggNER.[34,35] To investigate the involvement of Rev1 in tolerance of 4-oxo-2(E)-nonenal (4-ONE)-deoxycytidine, a prototypic helix-distorting hydroxyalkenal-nucleotide adduct (Figure 5B), we performed a quantitative in cellulo TLS assay.[33] Indeed, mutagenic TLS at the 4-ONE-cytidine adduct largely depended on Rev1 in MEFs (Figure 5C). Consistently, *Rev1* or *Xpc* and, to a greater extent, *Rev1Xpc* MEFs were hypersensitive to paraquat that induces oxidative stress by poisoning mitochondria (Figure 5D), whereas *Rev1Xpc* MEFs also were hypersensitive to 4-HNE, a compound closely related to 4-ONE (Figure 5E). Taken together, these data strongly suggest that a defect in Rev1-dependent TLS of persistent helix-distorting oxidative DNA lesions at the nuclear genome is responsible for the degenerative hematopoietic phenotypes of *Rev1* and *Rev1Xpc* mice.

Although a priori one would not expect overall cellular ROS levels to be increased in the absence of ggNER and TLS, we observed significant accumulation of the oxidative stress and aging marker lipofuscin[36] in bone marrow of *Rev1Xpc* mice (Figure 5F). Also intracellular levels of 4-HNE, as well as expression of the oxidative stress response marker phospho-p38,[37] were increased in *Rev1Xpc*, compared with *Xpc*, bone marrow cells (Figure 5G-H; supplemental Figure 6C). Consequently, also levels of oxidative DNA lesions at the genome were increased in *Rev1* and, to a greater extent, *in Rev1Xpc*, bone marrow, as demonstrated by staining for genomic 8OHdG (Figure 5I). Because 8OHdG is no substrate for ggNER, this result emphasizes that a de novo source of oxidative stress only indirectly is caused by the ggNER and TLS deficiency.

Progressive mitochondrial dysfunction and oxidative stress in *Rev1Xpc* HSPCs

The progressive increase of ROS levels in *Rev1Xpc* bone marrow suggested the emergence of a de novo source of oxidative stress in response to replication stress at helix-distorting nucleotide lesions. To investigate the origin of this phenomenon, we focused our attention to the mitochondrial compartment as the dominant source of

Figure 5. Rev1-dependent TLS and ggNER converge on helix-distorting oxidative DNA lesions resulting from progressive mitochondrial dysfunction (see also supplemental Figure 6). We investigated the involvement of Rev1-dependent TLS at helix-distorting lipid peroxidation–derived nucleotide adduct by treating *Rev1* HSCs with a radical scavenger, by using an in cellulo TLS assay, by investigating the sensitivity of *Rev1* cells to a lipid peroxidation–derived aldehyde, to oxidative stress, and by measuring oxidative stress in bone marrow. We then characterized the quantity and functionality of *Rev1Xpc* mitochondria. $^{*}P < .05$; $^{**}P < .01$; $^{***}P < .001$; $^{****}P < .0001$. Data are mean ± SEM. (A) DNA breaks (γH2AX) in cultured HSCs (LSK-SLAM), WT (n = 3), and *Rev1* (n = 3), treated or nontreated with the ROS scavenger NAC. The fraction of positive cells shown was normalized relative to WT. (B) The prototypic DNA-reactive lipid peroxidation–derived aldehyde 4-ONE and its adduction to a cytosine base (H-εdC). (C) Top: TLS assay at a site-specific H-εdC. MEFs were transfected with the substrate, followed by incubation to allow TLS, and by recovery of covalently closed progeny plasmids in *Escherichia coli*. The fraction of recovered substrate, compared with an undamaged internal control, is a measure of TLS activity of the MEFs. Bottom: Relative efficiency and mutation spectrum of TLS events at a site-specific H-εdC lesion. (D) Clonal survival of WT, *Rev1*, *Xpc*, and *Rev1Xpc* MEFs in response to the addition of the mitochondrial poison paraquat to the growth medium. (E) Clonal survival of *Xpc* and *Rev1Xpc* MEFs in response to the addition of 4-HNE to the growth medium. Oxidative stress in the bone marrow of *Rev1Xpc* mice as evidenced by: lipofuscin accumulation (brown inclusions) in bone marrow of moribund mice (F), 4-HNE-positive cells (G), activation of p38 signaling [phospho (γ)p38 staining] (H), and accumulation of free radical-induced oxidative DNA lesions (OHdG-positive cells) (I) in *Rev1Xpc* mice: 1m (n = 3-4), 3m (n = 3-5), MB (n = 5-6). The fraction of positive cells shown was normalized relative to 3-month-old WT bone marrow. (J) Relative mtDNA contents, as determined by real-time PCR, in bone marrow from *Xpc* (n = 5-6) and *Rev1Xpc* (n = 5-6) mice. All mtDNA levels were normalized to those in 3-month-old *Xpc* mice. (K) Western blot of mitochondrial complexes I to IV in bone marrow from *Xpc* and *Rev1Xpc* mice (4 mice per group). Lamin B1: internal standard. (L) Expression of the mitochondrial stress proteins UCP2 and PGC-1α in WT, *Xpc*, *Rev1*, and *Rev1Xpc* bone marrow. Lamin B: internal standard. wk, weeks; m, months; MB, moribund (see Figure 2C for survival data). (M) Mitochondrial membrane potentials in bone marrow of *Xpc* and *Rev1Xpc* mice. All potentials in *Rev1Xpc* bone marrow were normalized to those in *Xpc* bone marrow of the same age. 1 m (n = 4), 1.5 m (n = 4), 3 m (n = 4-6), MB (n = 3-4). (N) Basal oxygen consumption rates in viable cells from bone marrow from *Xpc* and *Rev1Xpc* mice. All oxygen consumption rates in *Rev1Xpc* bone marrow were normalized to those in *Xpc* bone marrow of the same age. 2wk (n = 5-6), 3 m (n = 3).

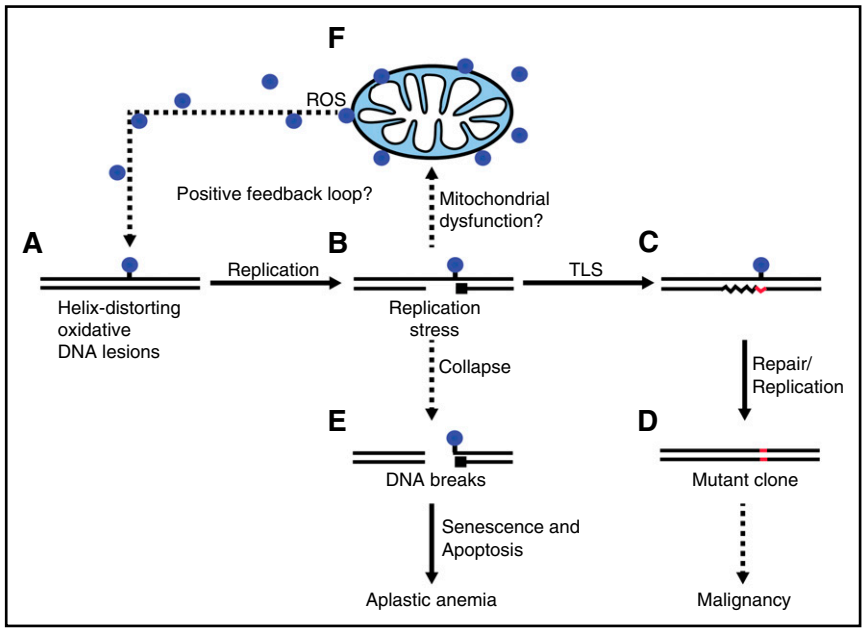

Figure 6. Model for the role of mutagenic TLS in maintenance of the hematopoietic system. (A) Genomic nucleotides, damaged by endogenous sources or by chemical decay, form a threat to DNA transactions such as transcription or replication, in case they remain unrepaired. (B) Processive replication is arrested by a nucleotide, damaged by a helix-distorting oxidative nucleotide lesion. (C) The damaged nucleotide is bypassed by TLS. This prevents replication stress, but at the expense of the frequent incorporation of an incorrect nucleotide opposite the lesion (in red). (D) Subsequent repair of the damaged nucleotide, or replication of the bottom DNA strand, fixates the mutation. This contributes to the acquisition of clonal mutations in the aging hematopoietic system. Mutations in hematopoietic cells acquired during aging have been associated with the development of myeloid neoplasms in humans. (E) Stalled replicons that are not released by TLS can collapse to dsDNA breaks. DNA damage signaling at ssDNA gaps opposing the lesions and at dsDNA breaks induces senescence or apoptosis, ultimately resulting in collapse of the hematopoietic system. (F) We hypothesize that failure to release arrested replicons may underlie the observed mitochondrial dysfunction, possibly via depletion of NAD^+ that is required simultaneously at DNA breaks and for mitochondrial respiration. This may lead to increased ROS production and to the induction of additional oxidative DNA lesions. A positive feedback loop between replication stress at the nuclear genome and mitochondrial dysfunction is proposed to further accelerate the collapse of the hematopoietic system.

intracellular ROS. Because mitochondrial proliferation is an early cellular stress cellular response,[38] we first quantified mitochondrial DNA and protein in bone marrow. Indeed, in bone marrow of 3-month-old *Rev1Xpc* mice, these amounts were significantly increased (Figures 5J-K; supplemental Figure 6D). This suggests that replication stress at endogenous nucleotide lesions may lead to mitochondrial proliferation.

The mitochondrial uncoupling protein UCP2, which is induced by 4-HNE,[39] and also the expression of the transcriptional coactivator PGC-1α, a key controller of mitochondrial biogenesis,[40,41] participate in the mitochondrial response to oxidative stress.[39,41,42] In bone marrow of *Rev1Xpc* mice, the expression of both mitochondrial proteins was strongly increased, consistent with the presence of chronic oxidative stress signaling (Figure 5L).

We then investigated mitochondrial function in bone marrow of all 4 genotypes. Compared with *Xpc* bone marrow, the mitochondrial membrane potential was attenuated in *Rev1Xpc* bone marrow, already at the age of 1 month (Figure 5M). Also in *Rev1* single-deficient mice, the mitochondrial membrane potential appeared to be reduced slightly, although this failed to reach significance (supplemental Figure 6G). In live bone marrow cells of 3-month-old *Rev1Xpc* mice, the basal, ATP-dependent, and reserve respiratory capacities in viable cells had virtually vanished (Figure 5N; supplemental Figure 6E-F). Although cell counts were reduced in *Rev1Xpc* bone marrow, the replication and proliferation of viable cells was not significantly different between the genotypes (Figures 4A-B,E; supplemental Figure 6G). This suggests that the mitochondrial proliferation and concomitant dysfunction may be a corollary of nuclear replication stress at the nuclear genome, originating the exacerbated ROS production in proliferating *Rev1Xpc* bone marrow cells.

Discussion

The attrition of tissues during aging is associated with the accumulation of oxidative and other endogenous DNA lesions at the nuclear genome of long-term stem and precursor cells.[5,17,18] However, the exact character of these lesions, their biological impact, the mechanistic basis of their cytotoxicity, and the pathways involved in pleiotropic responses to these damages have largely remained unexplored.[3] The effect of ROS on the genomic integrity of long-term HSCs is restrained by a hypoxic environment (the stem cell niche) and by a metabolically quiescent state, employing glycolysis rather than oxidative respiration.[37,43,44] This suggests that the exposure of HSCs to ROS negatively affects their function. Indeed, aging HSCs display DNA damage responses, although controversy exists about the nature of the underlying damage and whether the damage is induced during dormancy[45] or during proliferation.[46] Recently, the aging-associated decay of HSCs has been attributed to replication stress resulting from the decreasing expression of the minichromosome maintenance helicase.[47,48] Here we use *Rev1* mice to demonstrate that replication stress at helix-distorting oxidative DNA lesions at the nuclear genome is associated with the functional and genomic attrition of the hematopoietic system (Figures 1, 3, and 5; supplemental Figure 4). The hematopoietic phenotypes of *Rev1* mice are synergistically aggravated when, additionally, ggNER is compromised (resulting from the disruption of *Xpc*; Figures 2-4 and supplemental Figures 2-5). These data reveal that ggNER and TLS jointly preserve the genomic and functional integrity of the hematopoietic system by, respectively, repairing endogenous helix-distorting DNA lesions and suppressing replication stress at these lesions (Figure 6). The observation that loss of HSCs occurred during ontogeny, and

independent of tissue context (both in the prenatal liver and in postnatal bone), further confirms that these phenotypes are cell autonomous.

Mitochondrial dysfunction causes attrition of the hematopoietic system,[49,50] and a genomic DNA damage-dependent communication between the nucleus and mitochondria, leading to mitochondrial attrition, has been associated with aging-related pathologies.[38,51,52] Although Rev1 is not found in mitochondria,[53] viable *Rev1Xpc* and, to some extent, also *Rev1* bone marrow cells develop mitochondrial dysfunction suggesting that nuclear replication stress affects mitochondrial activity. In *Rev1* liver and cultured fibroblasts, mitochondrial dysfunction is associated with elevated activity of poly(ADP) ribose polymerase 1 (PARP1), possibly at ssDNA breaks. This presumably results in depletion of the PARP1 substrate and essential mitochondrial cofactor, NAD^+ (N.B.F., J. A. Durhuus, C. E. Regnell, M. Angleys, C. Desler, M. Hasan-Olive, A. Martin-Pardillos, A.T.-S., K. Thomsen, M. Laauritzen, V. A. Bohr, N.d.W., Bergensen, L.H., and L.J.R., submitted August 2017). A similar mechanism causes mitochondrial dysfunction in cells with a defect in the minor, transcription-coupled, NER subpathway.[54] We hypothesize that the increase in genomic replication stress, caused by ROS production by dysfunctional mitochondria, accelerates the collapse of the *Rev1Xpc* hematopoietic system (Figure 6F). Nevertheless, direct evidence for this hypothesis is lacking, and we cannot formally exclude that the mitochondrial dysfunction reflects, rather than originates, the decay of the *Rev1Xpc* bone marrow.

The decay of the hematopoietic system of *Rev1* and, to a greater extent, *Rev1Xpc* mice may represent dramatically accelerated hematopoietic aging. The hematopoietic phenotypes of *Rev1* single-deficient mice, and the finding that *Xpc* or *Rev1* single-deficient cells already display moderate sensitivity to UV light (supplemental Figure 2B), emphasize that ggNER and TLS are unable to either repair or bypass, respectively, all helix-distorting nucleotide lesions. We therefore hypothesize that the phenotypes of *Rev1* and *Rev1Xpc* bone marrow represent exacerbated phenotypes that contribute to the physiological functional attrition of HSCs in the aging bone marrow.[1,15] Also, small-chain endogenous aldehydes have been identified as a threat to the integrity of the hematopoietic system.[55,56] Therefore, multiple types of unreplicated endogenous DNA damage in parallel may participate in the aging-associated functional decline of the hematopoietic system. Nucleotide substitutions and inefficient DNA repair are strongly correlated with aging-associated hematopoietic and other malignancies.[6,16,57-61] Because Rev1-mediated TLS of damaged nucleotides, including lipid peroxidation–adducted nucleotides, is highly mutagenic (Figure 5B[9]), we hypothesize that the accumulation of such mutations is the price to pay for the protection of the hematopoietic system against endogenous helix-distorting oxidative nucleotide lesions by error-prone TLS. Finally, future investigations may also address the question of whether Rev1-mediated TLS is preserved, and perhaps provides a mechanism of survival, in leukemic cells and therefore represents a potential therapeutic target.

Acknowledgments

The authors acknowledge the skillful assistance of the personnel of the animal facilities and Mark Drost and Jacob G. Jansen for helpful comments on the manuscript. The authors thank Lemelinda Marques for assisting with mouse experiments.

A.M.-P., S.L., N.B.F., L.J.R., G.d.H., and N.d.W. were supported by an EU Marie Curie/ITN grant 316964 ("MARriAGE"). N.d.W. and A.T.-S. also received a grant from the Dutch Cancer Society (UL 2010-4851). G.d.H. and R.P.v.O. are supported by the Mouse Clinic for Cancer and Ageing, funded by a grant from The Netherlands Organization of Scientific Research. M.M. was supported by the National Institutes of Health, National Institute of Environmental Health Sciences (ES018833). B.v.L. was funded by the Swiss National Science foundation and the Onsager Fellowship. N.B.F. and L.J.R. additionally were supported by Nordea-fonden. M.H.G.P. R. was supported by grants from the Dutch Cancer Society, the Netherlands Organization of Scientific Research and the Netherlands Genomics Initiative.

Authorship

Contribution: M.M., L.J.R., G.d.H., M.H.G.P.R., and N.d.W. designed and supervised the experiments and interpreted the results; N.d.W. wrote the manuscript; A.M.-P., A.T.-S., S.C., S.L., R.P.v.O., A.D.-A., N.B.F., M.B., R.A., B.v.L., D.C.F.S., K.H., and C.D.-v.d.S. carried out experiments; and all authors edited the manuscript.

Conflict-of-interest disclosure: The authors declare no competing financial interests.

Correspondence: Niels de Wind, Leiden University Medical Center, Einthovenweg 20, 2333ZC Leiden, The Netherlands; e-mail: n.de_wind@lumc.nl; and Marc H. G. P. Raaijmakers, Department of Hematology, Erasmus Medical Center Cancer Institute, Rotterdam, The Netherlands; e-mail: m.h.g.raaijmakers@erasmusmc.nl.

References

1. López-Otín C, Blasco MA, Partridge L, Serrano M, Kroemer G. The hallmarks of aging. *Cell*. 2013; 153(6):1194-1217.
2. Swenberg JA, Lu K, Moeller BC et al. Endogenous versus exogenous DNA adducts: their role in carcinogenesis, epidemiology, and risk assessment. *Toxicol Sci*. 2011;120(suppl 1): S130-S145.
3. Mandal PK, Blanpain C, Rossi DJ. DNA damage response in adult stem cells: pathways and consequences. *Nat Rev Mol Cell Biol*. 2011;12(3): 198-202.
4. Blanpain C, Mohrin M, Sotiropoulou PA, Passegué E. DNA-damage response in tissue-specific and cancer stem cells. *Cell Stem Cell*. 2011;8(1):16-29.
5. Vitale I, Manic G, De Maria R, Kroemer G, Galluzzi L. DNA damage in stem cells. *Mol Cell*. 2017;66(3):306-319.
6. Marteijn JA, Lans H, Vermeulen W, Hoeijmakers JHJ. Understanding nucleotide excision repair and its roles in cancer and ageing. *Nat Rev Mol Cell Biol*. 2014;15(7):465-481.
7. Fischer JL, Kumar MAS, Day TW, et al. The Xpc gene markedly affects cell survival in mouse bone marrow. *Mutagenesis*. 2009;24(4):309-316.
8. Branzei D, Psakhye I. DNA damage tolerance. *Curr Opin Cell Biol*. 2016;40:137-144.
9. Sale JE, Lehmann AR, Woodgate R. Y-family DNA polymerases and their role in tolerance of cellular DNA damage. *Nat Rev Mol Cell Biol*. 2012;13(3):141-152.
10. Washington MT, Minko IG, Johnson RE, et al. Efficient and error-free replication past a minor-groove N2-guanine adduct by the sequential action of yeast Rev1 and DNA polymerase zeta. *Mol Cell Biol*. 2004;24(16):6900-6906.
11. Zhou Y, Wang J, Zhang Y, Wang Z. The catalytic function of the Rev1 dCMP transferase is required in a lesion-specific manner for translesion synthesis and base damage-induced mutagenesis. *Nucleic Acids Res*. 2010;38(15): 5036-5046.
12. Schiavone D, Guilbaud G, Murat P, et al. Determinants of G quadruplex-induced epigenetic instability in REV1-deficient cells. *EMBO J*. 2014; 33(21):2507-2520.
13. Roy U, Schärer OD. Involvement of translesion synthesis DNA polymerases in DNA interstrand crosslink repair. *DNA Repair (Amst)*. 2016;44: 33-41.
14. Biechonski S, Yassin M, Milyavsky M. DNA-damage response in hematopoietic stem cells: an evolutionary trade-off between blood regeneration and leukemia suppression. *Carcinogenesis*. 2017; 38(4):367-377.

15. Akunuru S, Geiger H. Aging, clonality, and rejuvenation of hematopoietic stem cells. *Trends Mol Med*. 2016;22(8):701-712.
16. Adams PD, Jasper H, Rudolph KL. Aging-induced stem cell mutations as drivers for disease and cancer. *Cell Stem Cell*. 2015;16(6):601-612.
17. Yahata T, Takanashi T, Muguruma Y, et al. Accumulation of oxidative DNA damage restricts the self-renewal capacity of human hematopoietic stem cells. *Blood*. 2011;118(11):2941-2950.
18. Porto ML, Rodrigues BP, Menezes TN et al. Reactive oxygen species contribute to dysfunction of bone marrow hematopoietic stem cells in aged C57BL/6 J mice. *J Biomed Sci*. 2015;22:97.
19. Jansen JG, Langerak P, Tsaalbi-Shtylik A, van den Berk P, Jacobs H, de Wind N. Strand-biased defect in C/G transversions in hypermutating immunoglobulin genes in Rev1-deficient mice. *J Exp Med*. 2006;203(2):319-323.
20. Dykstra B, Olthof S, Schreuder J, Ritsema M, de Haan G. Clonal analysis reveals multiple functional defects of aged murine hematopoietic stem cells. *J Exp Med*. 2011;208(13):2691-2703.
21. van Os RP, Dethmers-Aussema B, de Haan G. In vitro assays for cobblestone area-forming cells, LTC-IC, and CFU-C. *Methods Mol Biol*. 2008;430: 143-157.
22. Ploemacher RE, van der Sluijs JP, van Beurden CA, Baert MR, Chan PL. Use of limiting-dilution type long-term marrow cultures in frequency analysis of marrow-repopulating and spleen colony-forming hematopoietic stem cells in the mouse. *Blood*. 1991;78(10):2527-2533.
23. Turley H, Wykoff CC, Troup S, Watson PH, Gatter KC, Harris AL. The hypoxia-regulated transcription factor DEC1 (Stra13, SHARP-2) and its expression in human tissues and tumours. *J Pathol*. 2004;203(3):808-813.
24. McGlynn AP, Wasson G, O'Connor J, McKerr G, McKelvey-Martin VJ, Downes CS. The bromodeoxyuridine comet assay: detection of maturation of recently replicated DNA in individual cells. *Cancer Res*. 1999;59(23):5912-5916.
25. Hashimoto K, Cho Y, Yang I-Y, et al. The vital role of polymerase ζ and REV1 in mutagenic, but not correct, DNA synthesis across benzo[a]pyrene-dG and recruitment of polymerase ζ by REV1 to replication-stalled site. *J Biol Chem*. 2012; 287(12):9613-9622.
26. Jansen JG, Tsaalbi-Shtylik A, Hendriks G, et al. Separate domains of Rev1 mediate two modes of DNA damage bypass in mammalian cells. *Mol Cell Biol*. 2009;29(11):3113-3123.
27. Sears DA, Udden MM. Howell-Jolly bodies: a brief historical review. *Am J Med Sci*. 2012;343(5): 407-409.
28. Lukas C, Savic V, Bekker-Jensen S, et al. 53BP1 nuclear bodies form around DNA lesions generated by mitotic transmission of chromosomes under replication stress. *Nat Cell Biol*. 2011;13(3):243-253.
29. Sedelnikova OA, Horikawa I, Zimonjic DB, Popescu NC, Bonner WM, Barrett JC. Senescing human cells and ageing mice accumulate DNA lesions with unrepairable double-strand breaks. *Nat Cell Biol*. 2004;6(2):168-170.
30. Winterbourn CC, Kettle AJ, Hampton MB. Reactive oxygen species and neutrophil function. *Annu Rev Biochem*. 2016;85:765-792.
31. Kosinska W, Khmelnitsky M, Kim JH, Zhao Z-L, Guttenplan JB. Effects of potential dietary inhibitors of endogenous DNA damage on mutagenesis and lipid peroxidation in lacZ mice. *Environ Mol Mutagen*. 2011;52(6):502-509.
32. Wang J, Clauson CL, Robbins PD, Niedernhofer LJ, Wang Y. The oxidative DNA lesions 8,5′-cyclopurines accumulate with aging in a tissue-specific manner. *Aging Cell*. 2012;11(4): 714-716.
33. Nam T-G. Lipid peroxidation and its toxicological implications. *Toxicol Res*. 2011;27(1):1-6.
34. Kuraoka I, Bender C, Romieu A, Cadet J, Wood RD, Lindahl T. Removal of oxygen free-radical-induced 5′,8-purine cyclodeoxynucleosides from DNA by the nucleotide excision-repair pathway in human cells. *Proc Natl Acad Sci USA*. 2000;97(8): 3832-3837.
35. Choudhury S, Pan J, Amin S, Chung F-L, Roy R. Repair kinetics of trans-4-hydroxynonenal-induced cyclic 1,N2-propanodeoxyguanine DNA adducts by human cell nuclear extracts. *Biochemistry*. 2004;43(23):7514-7521.
36. Höhn A, Grune T. Lipofuscin: formation, effects and role of macroautophagy. *Redox Biol*. 2013; 1(1):140-144.
37. Jang Y-Y, Sharkis SJ. A low level of reactive oxygen species selects for primitive hematopoietic stem cells that may reside in the low-oxygenic niche. *Blood*. 2007;110(8): 3056-3063.
38. Quirós PM, Mottis A, Auwerx J. Mitonuclear communication in homeostasis and stress. *Nat Rev Mol Cell Biol*. 2016;17(4):213-226.
39. Mailloux RJ, Harper M-E. Uncoupling proteins and the control of mitochondrial reactive oxygen species production. *Free Radic Biol Med*. 2011; 51(6):1106-1115.
40. Lustig Y, Ruas JL, Estall JL, et al. Separation of the gluconeogenic and mitochondrial functions of PGC-1alpha through S6 kinase. *Genes Dev*. 2011;25(12):1232-1244.
41. Sahin E, Colla S, Liesa M, et al. Telomere dysfunction induces metabolic and mitochondrial compromise. *Nature*. 2011;470(7334):359-365.
42. St-Pierre J, Drori S, Uldry M, et al. Suppression of reactive oxygen species and neurodegeneration by the PGC-1 transcriptional coactivators. *Cell*. 2006;127(2):397-408.
43. Simsek T, Kocabas F, Zheng J, et al. The distinct metabolic profile of hematopoietic stem cells reflects their location in a hypoxic niche. *Cell Stem Cell*. 2010;7(3):380-390.
44. Parmar K, Mauch P, Vergilio J-A, Sackstein R, Down JD. Distribution of hematopoietic stem cells in the bone marrow according to regional hypoxia. *Proc Natl Acad Sci USA*. 2007;104(13): 5431-5436.
45. Beerman I, Seita J, Inlay MA, Weissman IL, Rossi DJ. Quiescent hematopoietic stem cells accumulate DNA damage during aging that is repaired upon entry into cell cycle. *Cell Stem Cell*. 2014;15(1):37-50.
46. Walter D, Lier A, Geiselhart A, et al. Exit from dormancy provokes DNA-damage-induced attrition in haematopoietic stem cells. *Nature*. 2015;520(7548):549-552.
47. Flach J, Bakker ST, Mohrin M, et al. Replication stress is a potent driver of functional decline in ageing haematopoietic stem cells. *Nature*. 2014; 512(7513):198-202.
48. Alvarez S, Díaz M, Flach J et al. Replication stress caused by low MCM expression limits fetal erythropoiesis and hematopoietic stem cell functionality. *Nat Commun*. 2015;6:8548.
49. Liu X, Zhang Y, Ni M, et al. Regulation of mitochondrial biogenesis in erythropoiesis by mTORC1-mediated protein translation. *Nat Cell Biol*. 2017;19(6):626-638.
50. Ansó E, Weinberg SE, Diebold LP, et al. The mitochondrial respiratory chain is essential for haematopoietic stem cell function. *Nat Cell Biol*. 2017;19(6):614-625.
51. Fang EF, Scheibye-Knudsen M, Chua KF, Mattson MP, Croteau DL, Bohr VA. Nuclear DNA damage signalling to mitochondria in ageing. *Nat Rev Mol Cell Biol*. 2016;17(5):308-321.
52. Passos JF, Nelson G, Wang C, et al. Feedback between p21 and reactive oxygen production is necessary for cell senescence. *Mol Syst Biol*. 2010;6(1):347.
53. Zhang H, Chatterjee A, Singh KK. Saccharomyces cerevisiae polymerase zeta functions in mitochondria. *Genetics*. 2006;172(4): 2683-2688.
54. Fang EF, Scheibye-Knudsen M, Brace LE, et al. Defective mitophagy in XPA via PARP-1 hyperactivation and NAD(+)/SIRT1 reduction. *Cell*. 2014;157(4):882-896.
55. Garaycoechea JI, Crossan GP, Langevin F, Daly M, Arends MJ, Patel KJ. Genotoxic consequences of endogenous aldehydes on mouse haematopoietic stem cell function. *Nature*. 2012;489(7417):571-575.
56. Langevin F, Crossan GP, Rosado IV, Arends MJ, Patel KJ. Fancd2 counteracts the toxic effects of naturally produced aldehydes in mice. *Nature*. 2011;475(7354):53-58.
57. Genovese G, Kähler AK, Handsaker RE, et al. Clonal hematopoiesis and blood-cancer risk inferred from blood DNA sequence. *N Engl J Med*. 2014;371(26):2477-2487.
58. Jaiswal S, Fontanillas P, Flannick J, et al. Age-related clonal hematopoiesis associated with adverse outcomes. *N Engl J Med*. 2014;371(26): 2488-2498.
59. McKerrell T, Park N, Moreno T, et al; Understanding Society Scientific Group. Leukemia-associated somatic mutations drive distinct patterns of age-related clonal hemopoiesis. *Cell Reports*. 2015;10(8): 1239-1245.
60. Welch JS, Ley TJ, Link DC, et al. The origin and evolution of mutations in acute myeloid leukemia. *Cell*. 2012;150(2):264-278.
61. Blokzijl F, de Ligt J, Jager M, et al. Tissue-specific mutation accumulation in human adult stem cells during life. *Nature*. 2016;538(7624):260-264.

2017 130: 1523-1534
doi:10.1182/blood-2017-01-764274 originally published online August 21, 2017

Genomic and functional integrity of the hematopoietic system requires tolerance of oxidative DNA lesions

Ana Martín-Pardillos, Anastasia Tsaalbi-Shtylik, Si Chen, Seka Lazare, Ronald P. van Os, Albertina Dethmers-Ausema, Nima Borhan Fakouri, Matthias Bosshard, Rossana Aprigliano, Barbara van Loon, Daniela C. F. Salvatori, Keiji Hashimoto, Celia Dingemanse-van der Spek, Masaaki Moriya, Lene Juel Rasmussen, Gerald de Haan, Marc H. G. P. Raaijmakers and Niels de Wind

Blood (print ISSN 0006-4971, online ISSN 1528-0020), is published weekly by the American Society of Hematology, 2021 L St, NW, Suite 900, Washington DC 20036.

Supplemental Data

Extended methods

Mice and cell lines.

Wild type, *Rev1*, *Xpc* and *Rev1Xpc* mouse cohorts (equal numbers of females and males) were obtained by crossing FVB and C57Bl/6 parents and the hybrid progeny was used for most experiments, including reconstitution of the bone marrow in *Rev1Xpc* mice. Transplantation experiments using *Rev1* animals were performed in the C57Bl/6 background. Hairless albino SKH-1 mice were used for measurement of sensitivity of the skin to artificial sunlight. MEF lines were obtained from 13.5-day embryos of the hybrid FVBxC57Bl/6 background and immortalized using the 3T3 protocol. Survival after exposure to 4HNE and short-wave UV (UVC) light were measured using clonogenic assays. All animal care and experimental procedures were approved by the animal ethics committees of the participating Institutes. Mice were maintained on a 12-hour light regimen, receiving chow and water *ad libitum*. If appropriate, mice were given an intra-peritoneal injection with Bromodeoxyuridine (BrdU; 40 μg) and/or ethynyl-2'-deoxyuridine (EdU; 200 μg) in PBS, one hour before killing using CO_2, to label replicating cells.

Whole blood analysis

For whole blood analysis, peripheral blood was collected in heparin-coated tubes and manually counted using a Bürker chamber. For the quantification of white blood cell ratios and Howell-Jolly bodies, blood smears were stained with Giemsa (Merck-Millipore). Blood of 1.5 months-old mice was analyzed using an animal blood counter (Scil Animal Care).

Hematopoietic stem cell (HSC) isolation for flow cytometry

Concentrations and origin of reagents used are depicted in Supplemental Table 1. Bone marrow from wild type and *Rev1* animals was isolated by crushing tibia, femur, pelvis, sternum and spine and, after lysing with erylysis buffer, stained with a cocktail of antibodies against lineage markers (B220 Alexa 700, CD3 Alexa 700, Gr-1 Alexa 700, Mac-1 Alexa 700 and Ter-119 Alexa 700), c-Kit Phycoerythrin, Sca-1 Pacific Blue, CD48 Alexa 647, CD150 PeCy7, CD34 FITC and EPCR-Biotin with secondary Streptavidin APCy7, all from Biolegend. LT-HSC (Lin-Sca+Kit+CD48-CD34-CD150+EPCR+) cells were isolated on Moflo Astrios or XDP (Beckman Coulter). For the analysis of chimaerism of blood, 250 ul of peripheral blood was lysed with erylysis buffer and stained for CD45.2 Phycoerythrin, CD45.1 Pacific Blue, CD3 APC, B220 FITC, Gr-1 PeCy7 and Mac-1 PeCy7. Samples were acquired on BD FACS Canto and analyzed using Kaluza software (Beckman Coulter).

Single cell colony assays and DNA damage stainings

Concentrations and origin of reagents used are described in Supplemental Table 1. Single long-term-HSCs were sorted into the inner 60-wells of round-bottom 96-well plates and cultured for two weeks in Iscove's modified Dulbecco's medium (IMDM) and 20% BIT9500 Serum Substitute (Stemcell technologies) supplemented with 10% fetal calf serum and 100ng/ml IL-11, 100ng/ml Flt3 and 300ng/ml SCF with or without 100μM N-acetylcysteine at 37°C and 5% CO_2. Colony sizes were scored at day 7 and day 14 at 50x magnification using an ocular cross on Zeiss Axiovert 25. At day 14, cells were collected for immunofluorescence staining of DNA damage markers. Cells were permeabilized in 0.5% Triton-X-100 for 5 minutes on ice and fixed with 2% formaldehyde for 15 minutes at room temperature. 2000-5000 cells per spot were seeded onto adhesion slides (VWR) and fixed with 4% formaldehyde for a further 5 minutes at room temperature. Cells were blocked for 60 minutes in 10% goat serum (Invitrogen) followed by primary antibody staining for γH2AX (Abcam) and 53BP1 (Novusbio) for 1-2 hours followed by secondary antibody staining with goat anti-rabbit alexa-488 (Invitrogen) for one hour and stained with DAPI (2 μg/ml) for 10 minutes at room temperature. Coverslips were mounted with ProLong Gold Antifade Reagent (Invitrogen, Molecular Probes). Samples were imaged using a 63x objective on a Zeiss M3 microscope.

Flow cytometry of γH2AX

Concentrations and origin of reagents used are depicted in Supplemental Table 1. Cells were permeabilized in 1% Triton-X-100 for ten minutes and fixed with 4% PFA for 30 minutes at room temperature. Up to 1 x 10^6 cells were blocked in 10% goat serum (Invitrogen) followed by primary antibody staining for γH2AX (Abcam) at 1:100 dilution for 1 hour. Cells were washed once in PBS + 0.2% BSA and incubated with secondary antibody goat anti-rabbit Alexa-488 (Invitrogen) at 1:100 dilution for half an hour. γH2AX fluorescence was measured on BD FACS Canto and analyzed on Flowjo.

Cobblestone Area-Forming Cell (CAFC) assay
The CAFC assay was performed as previously described [21,22].

Transplantation experiments
For competitive transplantation experiments, 200 wild type or *Rev1* littermate donor HSCs (together with 1.2x10^6 W41.SJL c-kit receptor-mutant whole bone marrow cells as competitors), or 5 million wild type or *Rev1* bone marrow cells were transplanted into lethally (9 Gy) irradiated B6.SJL by retro-orbital injection. Blood cell analysis was performed every 4-6 weeks post-transplantation. For secondary transplantation, CD54.2+ bone marrow cells from primary recipients were injected in the orbital sinus of lethally irradiated (9 Gy) B6.SJL mice [20]. Reconstitution of the hematopoietic system of 1.5-months-old *Rev1Xpc* mice was performed by injecting 5x10^6 *Xpc* bone marrow cells in the tail vein. The genotypes of the reconstituted hematopoietic system was analyzed every 4-6 weeks post-transplantation using multiplex PCR. Primer sequences are as follows: *Rev1* primers: forward: 5'-ATTGTGAGTCTCTAGCGTTTG-3', reverse: 5'-GCTGGAATTGAAATTCTAGG-3', KO allele: 5'-GCTTCCATTGCTCAGCGGTG-3'. *Xpc* primers: forward: 5'-GCTACTTTCTGGCTTACAGTTC-3', reverse: 5-'TTAGGGATTGCGTGCATAC-3', KO allele: 5'-CCTTCTTGACGAGTTCTTCT-3'.

HSPC immunophenotyping, cell cycle and apoptosis analysis from *WT, Rev1, Xpc* and *Rev1Xpc* mice
Bone marrow from mice of all four genotypes was freshly isolated and the erythrocytes were lysed with ACK lysing buffer for 4 minutes on ice (Lonza, 10-548E). All antibody incubations for cell surface staining were performed in PBS+0.5% FCS for 20 min on ice in the dark. To identify HSPCs, we first stained the bone marrow cells with a cocktail (1:25) of biotin-labeled antibodies against the following lineage (Lin) markers: Gr1 (RB6-8C5), Mac1 (M1/70), Ter119 (TER-119), CD3e (145-2C11), CD4 (GK1.5), CD8 (53-6.7) and B220 (RA3-6B2) (all from BD Biosciences). Cells were then incubated with Pacific Orange-conjugated streptavidin (Life Technologies) and the following antibodies: Sca1 PB (D7), CD48 FITC or PE (HM48-1), CD150 PE-Cy7 (TC15-12F12.2) (all 1:100 dilution, all from Biolegend), c-Kit APC (1:100, BD Biosciences, 2B8) after the washing step. To identify stromal cells, bone fraction cell suspension was obtained after 45 minutes collagenase (Stem Cell Technology) incubation at 37°C and then was stained with the following antibodies: CD45.2 APC-Cy7 (104) (1:200), Ter119 BV510 (TER-119) (1:100), CD105 PE-Cy7 (MJ7/18) (1:100), CD51 PE (RMV-7) (1:50), Sca1 PB (D7) (1:100) (all from Biolegend), CD31 PE-CF594 (1:100) (MEC 13.3, BD Biosciences). 7AAD (1:100) (Beckman coulter, Stem-Kit Reagents IM3630) was added to the cell suspension prior analysis to exclude dead cells. All FACS data were acquired using a LSR II Flow Cytometer (BD) and analyzed with FlowJo 7.6.5 software (Tree Star).

Fetal *Xpc* and *Rev1Xpc* livers were analyzed 4 hours after BrdU injection of the mother. Fetal livers were treated with ACK lysing buffer (Lonza, 10-548E) prior to FACS analysis. The cell suspension was first stained with cell surface markers for HSPCs (see above), followed by BrdU staining using the FITC BrdU Flow Kit (BD Biosciences, 559619) according to the manufacturer's instructions. For the analysis of proliferating cells, freshly isolated fetal liver cells were first stained with HSPCs cell surface markers and then fixed and permeabilized using the Cytofix/Cytoperm kit (BD Biosciences, 554714). Cells were then incubated with Ki67 PE antibody (1:5, BD Bioscience, 556027) in 1x Perm/Wash buffer (BD Biosciences, 554723) for 20 minutes on ice and then washed. 7AAD (1:50) was added in the cell suspension to stain DNA prior to analysis. Apoptosis was assayed with APC Annexin V Apoptosis Detection Kit I (BD Biosciences) according to the recommendation of the

manufacturer. Dead cells were detected based on 7AAD staining. A BD LSR II flow cytometer was used for BrdU, Ki67 and Annexin analysis and FlowJo 7.6.5 software (Tree Star) was used to process the raw data.

Bone marrow extraction for stainings.
Bone marrow cells were extracted by flushing femurs and tibia. One intact femur was used to calculate bone marrow cellularities. The cell numbers were normalized to the body weight of individual mice. For stainings, legs were fixed overnight in 4% Formalin. Bones were decalcified by immersion using Kristensen decalcifier during 8 days. Paraffin-embedded sections were stained with Haematoxylin and Eosin (HE). Pathological examination was performed on coded samples.

Immunohistochemistry and immunofluorescence
Cells were permeabilized in 0.5% Triton-X-100 for 5 minutes on ice and fixed with 2% formaldehyde for 15 minutes at room temperature. Cells were seeded onto adhesion slides pre-treated with Poly-L-lysine solution (Sigma-Aldrich, P8920) by centrifugation in a Shandon Cytospin centrifuge and fixed with 4% formaldehyde for a further 5 minutes at room temperature. Cells were blocked for 60 minutes in 10 % goat serum (Invitrogen) or BSA 3% followed by primary antibody staining for 1 hour for BrdU/IdU (1:100, BD-bioscience, 347580), Caspase-3 (1:400, Cell Signaling, 9664), Dec1 (1:2000) [61], γ-H2AX (1:2000, Abcam, ab2893), Ki67 (1:1000, Abcam, ab15580), p16 (1:2000, Santa Cruz biotech, sc-1661), 8OHdG (1:200, Abcam, ab48508), phospho-p38 (1:100, Thermo Fisher, F.52.8), 53BP1 (1:1000, Novusbio, NB100-304); followed by secondary antibody staining with goat anti-rabbit or anti-mouse, Alexa-488 or Alexa-555 (1:1000, Invitrogen) for one hour. Coverslips were mounted with VectaShield mounting medium containing DAPI (Vector Laboratories, H-100). Samples were imaged using a 40x oil-immersion objective on a Zeiss Axio Imager M2 microscope.
Staining protocols for DNA damage markers in cultures LT-HSC from single cell colony assays were as described above. Coverslips were mounted with ProLong Gold Antifade Reagent (Invitrogen, Molecular Probes). Samples were imaged using a 63x objective on a Zeiss M3 fluorescence microscope. Staining for incorporated EdU was performed according to the manufacturers' instructions (Click-iT EdU Imaging Kit, Invitrogen, MP 10338). Annexin V staining was performed according to the manufacturer's (BD) protocol.

Bone marrow sections were deparaffinized using xylene and rehydrated in decreasing concentrations of ethanol. After rinsing in water, antigen retrieval was performed using a microwave oven in 0.01 M citrate buffer pH 6 during 10 minutes. Non-specific binding was blocked with Mouse IgG blocking reagent-MOM kit (Vector Laboratories. BMK-2202). The sections were treated with avidin/biotin (Vector Laboratories, SP-2001), following with primary antibody staining against 4-hydroxynonenal (4-HNE) for 1 hour at room temperature (1:100, Japan Institute for the control of Aging, MHN-100P). After washing the sections were incubated with biotinylated mouse IgG reagent (secondary antibody; 1:200, from the MOM kit) for 30 min. at room temperature. The sections were incubated with 0.9% H_2O_2 in water during 30 min to quench endogenous peroxidase. After washing sections were incubated with AB-complex for 30 min at room temperature (Vector Laboratories, PK-6101). The stain was then developed using NovaRed solution (Vector Laboratories, SK4800) and counterstained with Mayers hemalum (nuclear stain; LAMB/170-D, Raymond A Lamb) and mounted with DPX mountant (Sigma).

Alkaline Comet assays
Alkaline comet assays and staining for incorporated BrdU were performed on bone marrow cell suspensions, essentially as described [23]. Analysis was performed using the Comet Assay IV (Perceptive Instruments) system. Per condition at least 200 cells were analysed.

Translesion synthesis assay
The generation of a site-specific single-stranded H-εdC lesion and the determination of the efficiency and mutagenicity of TLS were performed essentially as described for a benzo[a]pyrene-dG adduct [24], see Figure 4E. Briefly, MEFs were cotransfected with a 'damage' plasmid containing a site-specific H-εdC lesion with an opposing gap, and with an undamaged internal control plasmid. After 3 days

progeny plasmids were recovered from cells by Hirt extraction, treated with Dpn1 that cleaves methylated (unreplicated) DNA, followed by recovery by transformation of *Escherichia coli.* The ratio between recovered damaged and undamaged plasmids serves to quantify the efficiency of TLS. The mutagenicity of the H-εdC lesion was determined by sequence analysis of recovered 'damaged' plasmids.

Mitochondrial membrane potential measurements

Mitochondrial membrane potentials were measured using MitoPT TMRE & TMRM Assay Kits (ImmunoChemistry Technologies, 9105). Controls for loss of membrane potential were performed by incubating bone marrow cells with 50 μM of the mitochondrial membrane depolarizer Carbonyl cyanide *m*-chlorophenyl hydrazone (CCCP) during 60 min at 37ºC in a CO_2 incubator. Bone marrow cells were stained with 200 nM MitoPT working solution during 20 min at 37º C. 7-Aminoactynomycin D (7AAD, 1:500; Thermofisher) was added to the cell suspension to enable to exclude dead cells prior to analysis. A Guava FACS flow cytometer was used for analysis and InCyte™ and GuavaSuite Software was used to process the raw data.

Bioenergetics

Freshly isolated total bone marrow cells were seeded and attached to XF 96 plate (Seahorse Bioscience) pretreated with Cell-Tak (Corning; Cat#354240). Respiration was analyzed using a Seahorse extracellular flux bioanalyzer (XF96; Seahorse Bioscience Inc.) and the XF Cell Mito Stress Test Kit according to manufacturer's instructions. Mitochondrial respiration was determined under normal conditions (Basal respiration) and following sequential injections of oligomycin (1 μM), carbonyl cyanide 4-(trifluoromethoxy) phenylhydrazone (FCCP, 3μM) and antimycin A (1 μM) to measure ATP–linked respiration, maximal respiration, and non-mitochondrial respiration, respectively. Proton leak and reserve respiratory capacity were calculated using these parameters and basal respiration.

Western blotting

Freshly frozen bone marrow cells were re-suspended in RIPA buffer (Sigma) supplemented with complete™, EDTA-free Protease Inhibitor Cocktail (Sigma) and PhosSTOP phosphatase inhibitor Cocktail (Sigma). The cell suspension was incubated on ice for 30 minutes followed by sonication (3x4 seconds). Then, the lysate was incubated on ice for another 10 minutes and centrifuged at 20K G-force for 20 minutes. The supernatant was mixed with NuPAGE® LDS Sample Buffer (4X) (Thermo Fisher Scientific). For gel electrophoresis, samples were heated to 50°C for 10 minutes and 15 μg protein was loaded on NuPAGE™ Novex™ 4-12% Bis-Tris Protein Gels, 1.0 mm (Thermo Fisher Scientific) and run according to the manufacturer's instruction. Antibodies that used: PGC1-α (Novus Biologicals, NBP1-04676), UCP2 (LifeSpan Bioscience, Inc., LS-B3249), Total OXPHOS Rodent WB Antibody Cocktail (Abcam, ab110413), Lamin B1 (Abcam, ab133741).

Isolation of genomic DNA and RNA

Genomic DNA (gDNA), RNA and Proteins were extracted from snap frozen tissues in liquid nitrogen, using Norgen Biotik RNA/DNA Purification Kit (Cat. 48700) according to the manufacturer's protocol.

Determination of relative mitochondrial (mt)DNA levels

Quantitative PCR (two independent reactions) was used for the measurement of mtDNA using SYBR Green PCR Master mix (Applied Biosystems). The mtDNA copy number was normalized to nuclear DNA by calculating the ratio of the mitochondrial DNA encoding the leucine 1 tRNA (Trnl1) to the nuclear Beta-2 microglobulin (B2m) gene. The following primers were used: B2m forward, 5′-GTCAGATATGTCCTTCAGCAAG-3′, and reverse, 5′-CTTAAACTCTGCAGGCGTATG-3′; and Trnl1 forward, 5′-AAGGTTATTAGGGTGGCAG-3′, and reverse, 5′-GGACGAGGAGTGTTAGGATA-3′.

For PCR reactions, 5 ng of genomic DNA was mixed with 2 μl of each primers (5 μM), 10 μl SYBR green and 0.4 μl ROX and nuclease free water to the final volume of 20 μl. The reaction was initiated

at 94°C. All reactions were run in triplicates. The relative mtDNA levels were calculated using formula $2\times2^{\Delta CT}$.

Supplemental Table 1. Antibodies used for flow cytometry and cell sorting.

Reagent	Supplier	Clone	Concentration	Reference
Alexa Fluor® 647 anti-mouse CD48 Antibody	Biolegend	HM48-1	0.5 mg/ml (used 1.4 µg per 10^8 cells)	103416
PE anti-mouse CD117 (c-Kit) Antibody	Biolegend	2B8	0.2 mg/ml (used 0.8 µg per 10^8 cells)	105808
PE/Cy7 anti-mouse CD150 (SLAM) Antibody	Biolegend	TC15-12F12.2	0.2 mg/ml (used 1.2 µg per 10^8 cells)	115914
Pacific Blue™ anti-mouse Ly-6A/E (Sca-1) Antibody	Biolegend	D7	0.5 mg/ml (used 1.4 µg per 10^8 cells)	108120
Alexa Fluor® 700 anti-mouse/human CD45R/B220 Antibody	Biolegend	RA3-6B2	0.5 mg/ml (used 0.6 µg per 10^8 cells)	103232
Alexa Fluor® 700 anti-mouse TER-119/Erythroid Cells Antibody	Biolegend	TER-119	0.5 mg/ml (used 2.3 µg per 10^8 cells)	116220
Alexa Fluor® 700 anti-mouse/human CD11b Antibody	Biolegend	M1/70	0.5 mg/ml (used 2.9 µg per 10^8 cells)	101222
Alexa Fluor® 700 anti-mouse CD3 Antibody	Biolegend	17A2	0.5 mg/ml (used 1.7 µg per 10^8 cells)	100216
Alexa Fluor® 700 anti-mouse Ly-6G/Ly-6C (Gr-1) Antibody	Biolegend	RB6-8C5	0.5 mg/ml (used 1.2µg per 10^8 cells)	108422
Anti-mouse EPCR biotin	Stem Cell Technologies	RMEPCR1560	0.2 mg/ml (used 1.2 µg per 10^8 cells)	10156
Streptavidin APC/Cy7	Biolegend		0.2 mg/ml (used 0.6 µg per 10^8 cells)	405208
CD34 FITC	BD Biosciences	RAM34	0.5 mg/ml (used 5 µg per 10^8 cells)	560238
PE anti-mouse CD45.2 Antibody	Biolegend	104	1:300	109808
Pacific Blue™ anti-mouse CD45.1 Antibody	Biolegend	A20	1:1400	110722
APC anti-mouse CD3 Antibody	Biolegend	145-2C11	1:350	100312
FITC anti-mouse/human CD45R/B220 Antibody	Biolegend	RA3-6B2	1:2500	103206
PE/Cy7 anti-mouse/human CD11b Antibody	Biolegend	M1/70	1:10.000	101216
PE/Cy7 anti-mouse Ly-6G/Ly-6C (Gr-1) Antibody	Biolegend	RB6-8C5	1:10.000	108416

Supplemental Table 2. Bone marrow cellularity and peripheral blood analysis of 1.5-months-old *Xpc* and *Rev1Xpc* mice.

Genotype (gender)	Weight (g)	BM cellularity (cells/ femur/g)	Ratio WBC/ erythrocy-tes	Total blood cells (cells/ml)	Erythro-cytes (cells/ml)	WBC (cells/ml)	Lympho-cytes (cells/ml)	Mono-cytes (cell/ml)	Granulo-cytes (cell/ml)	HGB (mmol/l)	HCT (l/l)	PLT (cells/ml)	MCV (fl)	MCH (fmol)	MCHC (mmol/l)	RDW (L%)	MPV (fl)
Xpc (M)	23,87	7,68E+05	0,00079	1,13E+10	1,13E+10	8,90E+06	7,70E+06	2,00E+05	1,00E+06	11,4	0,610	1,49E+08	54	1,01	18,7	11,8	6,4
Xpc (F)	20,3	1,24E+06	0,00104	1,07E+10	1,07E+10	1,11E+07	9,10E+06	3,00E+05	1,70E+06	10,8	0,559	1,83E+08	52	1	19,3	11,7	6,7
Xpc (M)	28,31	6,46E+05	0,00100	9,91E+09	9,90E+09	9,90E+06	7,70E+06	2,00E+05	2,00E+06	11,4	0,506	6,74E+08	53	1,19	22,5	11,7	5,4
Xpc (M)			0,00075	9,68E+09	9,67E+09	7,30E+06	5,50E+06	3,00E+05	1,40E+06	10,7	0,517	6,77E+08	54	1,11	20,75	11,8	6,55
Xpc (F)			0,00239	9,61E+09	9,59E+09	2,29E+07	1,67E+07	1,00E+06	5,50E+06	11,5	0,519	7,31E+08	54	1,21	22,4	11,8	6,1
Rev1Xpc (M)	20,39	8,17E+04	0,00068	7,81E+09	7,80E+09	5,30E+06	4,80E+06	0,00E+00	5,00E+05	9,3	0,475	1,27E+08	61	1,2	19,7	13,9	7,0
Rev1Xpc (F)	14,94	2,86E+05	0,00062	3,74E+09	3,74E+09	2,30E+06	2,00E+06	0,00E+00	3,00E+05	4,4	0,214	4,09E+08	57	1,18	20,7	14	6,4
Rev1Xpc (M)	23,23	1,67E+05	0,00100	5,98E+09	5,97E+09	5,97E+06	5,30E+06	1,00E+05	1,00E+06	8,2	0,362	3,22E+08	61	1,37	22,6	15,9	7,4
Rev1Xpc (M)	23,95	1,39E+05	0,00077	4,42E+09	4,42E+09	3,40E+06	2,95E+06	0,00E+00	4,50E+05	6,15	0,266	2,04E+08	60	1,39	23,1	15,8	7,05
Average *Xpc*	**24,16**	**8,84E+05**	**0,00089**	**1,02E+10**	**1,02E+10**	**9,30E+06**	**7,50E+06**	**2,50E+05**	**1,53E+06**	**1,11E+01**	**0,55**	**4,21E+08**	**53,25**	**1,08**	**20,31**	**11,75**	**6,26**
Average *Rev1Xpc*	**20,62**	**1,68E+05**	**0,00077**	**5,49E+09**	**5,48E+09**	**4,24E+06**	**3,76E+06**	**2,50E+04**	**5,63E+05**	**7,01E+00**	**0,33**	**2,65E+08**	**59,75**	**1,28**	**21,53**	**14,89**	**6,96**

Bone marrow was isolated by crushing the femur and cells were counted after lysis of the erythrocytes. Bone marrow cellularity was calculated dividing the total number of bone marrow cells by the animal weight (g). Whole blood analysis was performed using peripheral blood, collected by intracardial extraction and brief storage in heparin-coated tubes. Blood was analyzed using an animal blood counter (Scil Animal Care). BM (Bone Marrow), WBC (White Blood Cells), HGB (Hemoglobin), HCT (Hematocrit), PLT (Platelets), MCV (Mean Corpuscular Volume, also called Mean Cell Volume), MCH (Mean Corpuscular Hemoglobin), MCHC (Mean Corpuscular Hemoglobin Concentration), RDW (Red blood cell distribution width), MPV (Mean platelet volume).

Supplemental Figures

SUPPLEMENTAL FIGURE 1. Rev1 is required to maintain HSC function.

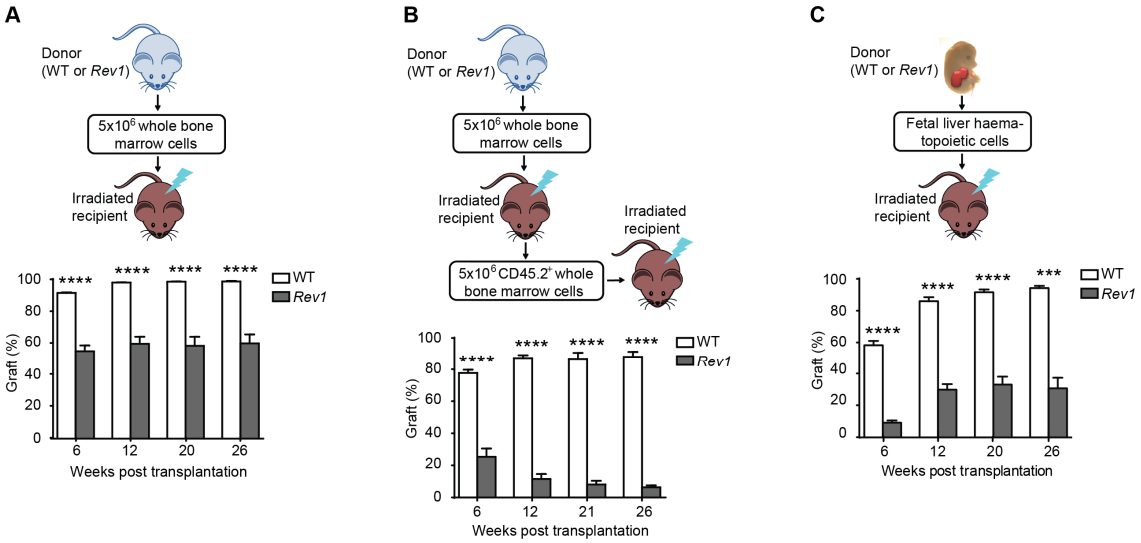

*p < 0.05. **p <0.01. ***p <0.001. ****p <0.0001. Data are mean ± S.E.M.

A. Mononuclear bone marrow cells (CD45.2) of 5-month old *Rev1* (n=10) or WT (n=15) mice were transplanted into CD45.1 recipients in a non-competitive fashion. Lower panel: Contribution of CD45.2 cells to hematopoiesis at different time points after transplantation indicating a reduced reconstitution ability of *Rev1*-deficient cells.

B. Serial transplantations of bone marrow mononuclear cells from the experiment described in Supplemental Figure 1B indicating progressive loss of *Rev1*-deficient HSC contribution to hematopoiesis upon secondary transplantation (n=9).

C. Non-competitive transplantation of hematopoietic cells from foetal liver of *Rev1* (n=5) and WT (n=5) mice demonstrating reduced repopulation capacity of *Rev1* cells.

SUPPLEMENTAL FIGURE 2. ggNER and TLS synergize to protect the hematopoietic system from attrition induced by helix-distorting DNA damage.

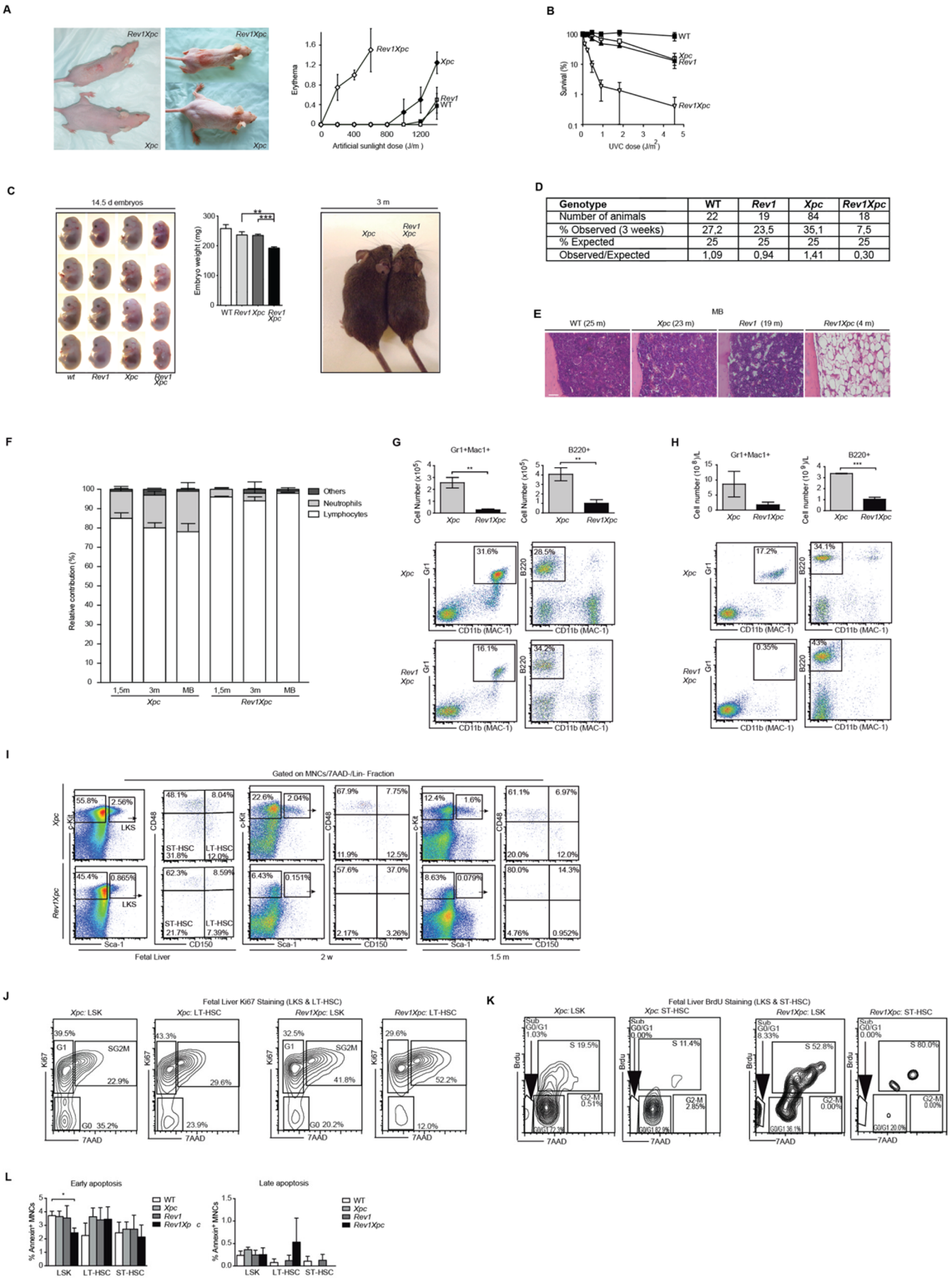

Genotype	WT	*Rev1*	*Xpc*	*Rev1Xpc*
Number of animals	22	19	84	18
% Observed (3 weeks)	27,2	23,5	35,1	7,5
% Expected	25	25	25	25
Observed/Expected	1,09	0,94	1,41	0,30

*p < 0.05. **p <0.01. ***p <0.001. ****p <0.0001. Data are mean ± S.E.M.

A. Increased sensitivity of *Rev1Xpc* mice to nucleotide lesions induced by UV light. Left panel: erythema induced by exposing the back of *Rev1Xpc* SKH-1 (hairless albino) mice to 1 cm^2-sized patches of artificial sunlight. Right panel: Quantification of responses of on the back of WT, *Rev1*, *Xpc* and *Rev1Xpc* SKH-1 mice to artificial sunlight.

B. Clonal survival of MEFs following short-wave UV (UVC) treatment that induces only helix-distorting nucleotide lesions.

C. Smaller mid-gestation size of *Rev1Xpc* embryos (left panel) and heir weight (middle panel). Right panel: Decreased size of adult *Rev1Xpc* mice.

D. Sub-Mendelian birth ratios of *Rev1Xpc* mice. Wild type (WT) and $Rev1^{-/-}$ mice were obtained from crosses between $Rev1^{+/-}$ parents. $Xpc^{-/-}$ and $Rev1^{-/-}Xpc^{-/-}$ mice were derived from crosses between $Rev1^{+/-}Xpc^{-/-}$ parents.

E. Aplasia of the bone marrow in moribund *Rev1Xpc* mice. Representative images of Hematoxylin-Eosin staining of paraffin-embedded sections of the femur of moribund mice of all four genotypes: Representative images of WT (n=5), *Xpc* (n=6), *Rev1* (n=7), *Rev1Xpc* (n=3). Bar size: 50 μM.

F. Relative contribution of myeloid and lymphoid cells in the *Rev1* and *Rev1Xpc* blood (n=10) at 3 time points.

G. Numbers of $Gr1^+Mac^+$ myeloid and $B220^+$ lymphoid, 7AAD-negative, cells in the bone marrow of *Xpc* and *Rev1Xpc* mice (upper panels) and representative FACS plots (lower panels).

H. Numbers of $Gr1^+Mac^+$ myeloid and $B220^+$ lymphoid, 7AAD-negative mononuclear, cells in the peripheral blood of *Xpc* and *Rev1Xpc* mice. Cell number quantification (left panels) and representative FACS plots (right panel).

I. Representative FACS plots showing the stem and progenitor cells (within the Lin^- fraction) in the fetal liver, in 2 weeks old and in 1.5 months old *Xpc* and *Rev1Xpc* mice. LKS: $Lin^-cKit^+Sca\text{-}1^+$ cells; ST-HSC: short-term hematopoietic stem cells ($Lin^-cKit^+Sca\text{-}1^+CD48^-CD150^-$ cells); LT-HSC: long-term hematopoietic stem cells ($Lin^-cKit^+Sca\text{-}1^+CD48^-CD150^+$).

J. Representative FACS plots showing Ki67/AAD staining of the LSK and ST-HSC fractions of the *Xpc* and *Rev1Xpc1* fetal liver cells.

K. Representative FACS plots showing Brdu/7AAD staining of the LSK and ST-HSC fraction of the *Xpc* and *Rev1Xpc1* fetal liver cells.

L. Early and late apoptosis (Annexin-V staining) in fetal liver HSC populations of all four genotypes.

SUPPLEMENTAL FIGURE 3. Hematopoietic defects of *Rev1Xpc* mice are cell-autonomous.

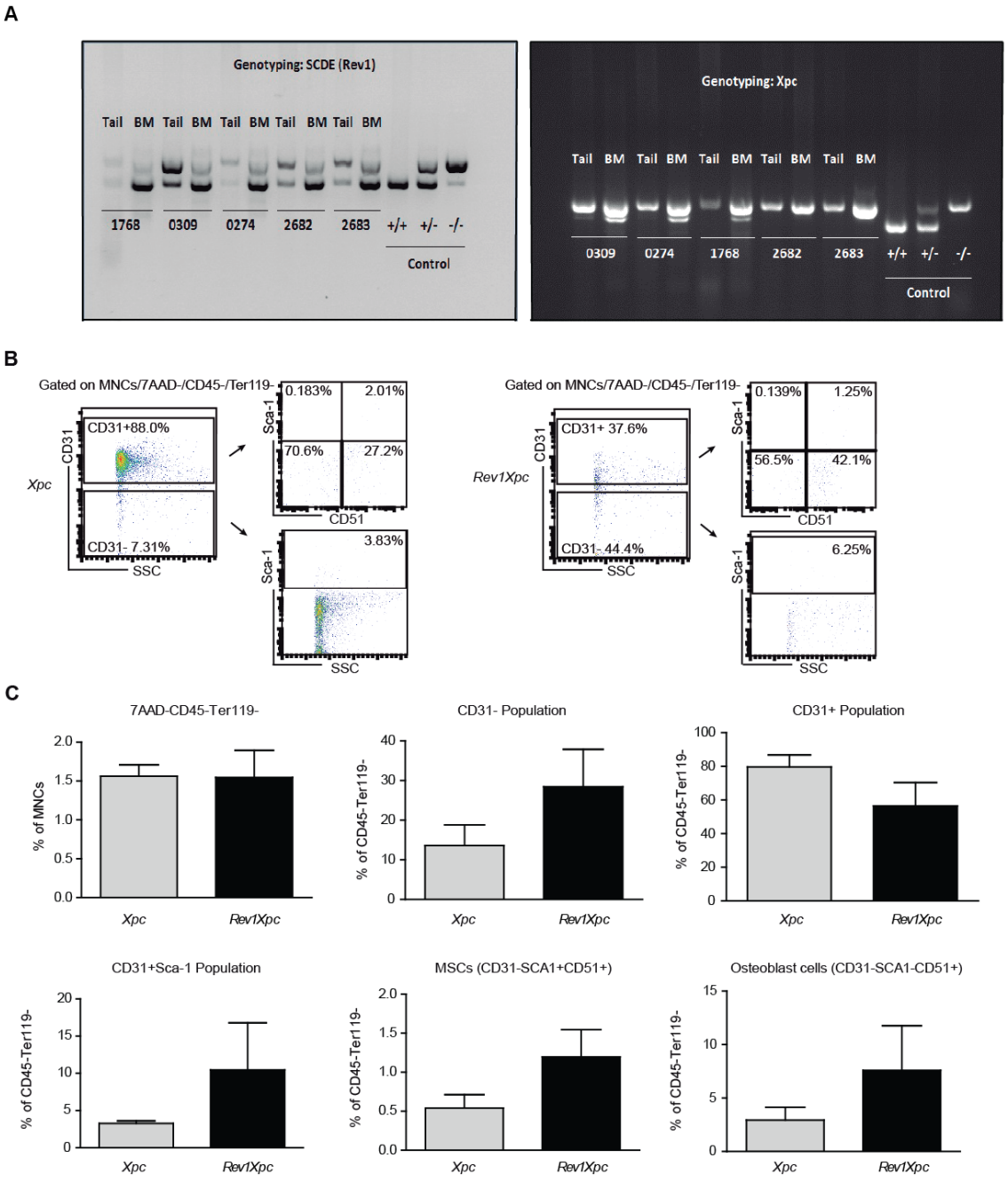

A. Donor-derived hematopoiesis following transplantation of 1.5-month old *Rev1Xpc* mice with *Xpc* marrow. Genotyping by PCR of tail and bone marrow-derived DNA of *Rev1Xpc* mice (n=5) (isolated at death), reconstituted with *Xpc* bone marrow. Left panel: PCR of DNA, showing gain of Rev1+/+ signal specifically in the bone marrow. Right panel: PCR confirming *Xpc* deficiency for both the soma (tail) and bone marrow.

B. Representative FACS plots of niche populations in *Xpc* (n=4) and *Rev1Xpc* mice (n=4) of 1.5 months old, indicating preservation of the niche composition in *Rev1Xpc* mice.

C. Relative frequencies of niche populations in *Xpc* (n=4) and *Rev1Xpc* mice (n=4) of 1.5 months old, indicating preservation of the niche composition in *Rev1Xpc* mice.

SUPPLEMENTAL FIGURE 4. TLS provides protection against ROS-induced replication stress and DNA breaks.

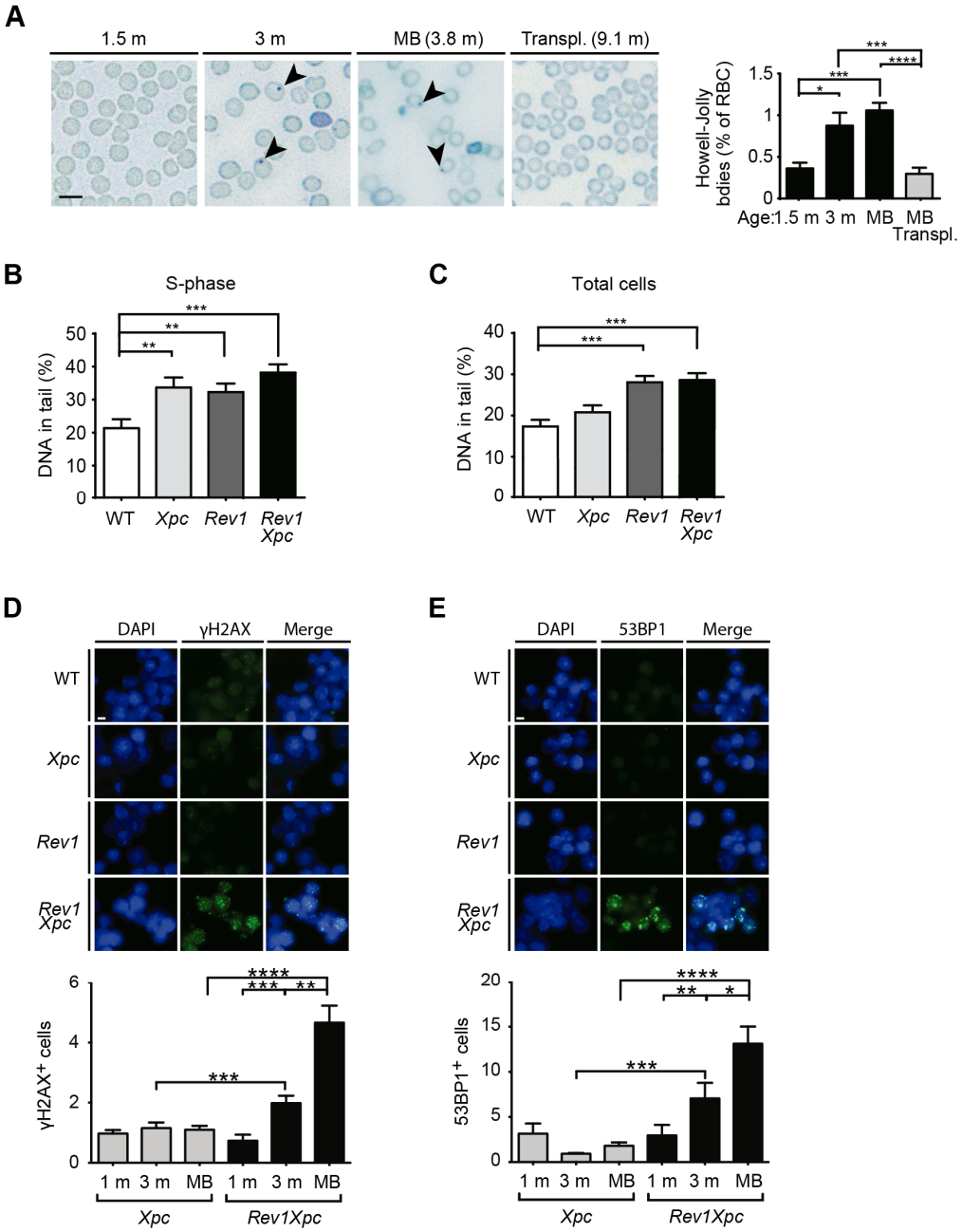

WT: (n=4-9), *Xpc*: (n=5-8), *Rev1*: (n=6), *Rev1Xpc*: (n=3-6). *p < 0.05. **p <0.01. ***p <0.001. ****p <0.0001. Data are mean ± S.E.M.

A. Left panel: Howell-Jolly bodies in non-transplanted versus transplanted *Rev1Xpc* mice. Right panel: quantification of Howell-Jolly bodies [1.5 m (n=6), 3 m (n=6), MB (n=8) and BM-transplanted (n=7)].

B. Chromosome breaks during S phase, measured by single-cell alkaline Comet gelelectrophoresis of bone marrow of 3 months old mice (n=4). Tail intensities of Bromodeoxyuridine-positive (S phase-positive) cells are shown here.

C. Chromosome breaks in bone marrow mononuclear cells, measured by single-cell alkaline Comet gel electrophoresis, in 3 months old mice (n=4).

D, E. Top panels: representative staining for DNA breaks (γH2AX; D, and 53BP1; E) in 3 months old bone marrow cells. Bottom panels: quantification of γH2AX staining in *Xpc* and *Rev1Xpc* bone marrow cells at the age of 1 and 3 months, and at death (MB).

SUPPLEMENTAL FIGURE 5. Rev1 protects against endogenous DNA damage-induced senescence and apoptosis in the hematopoietic system.

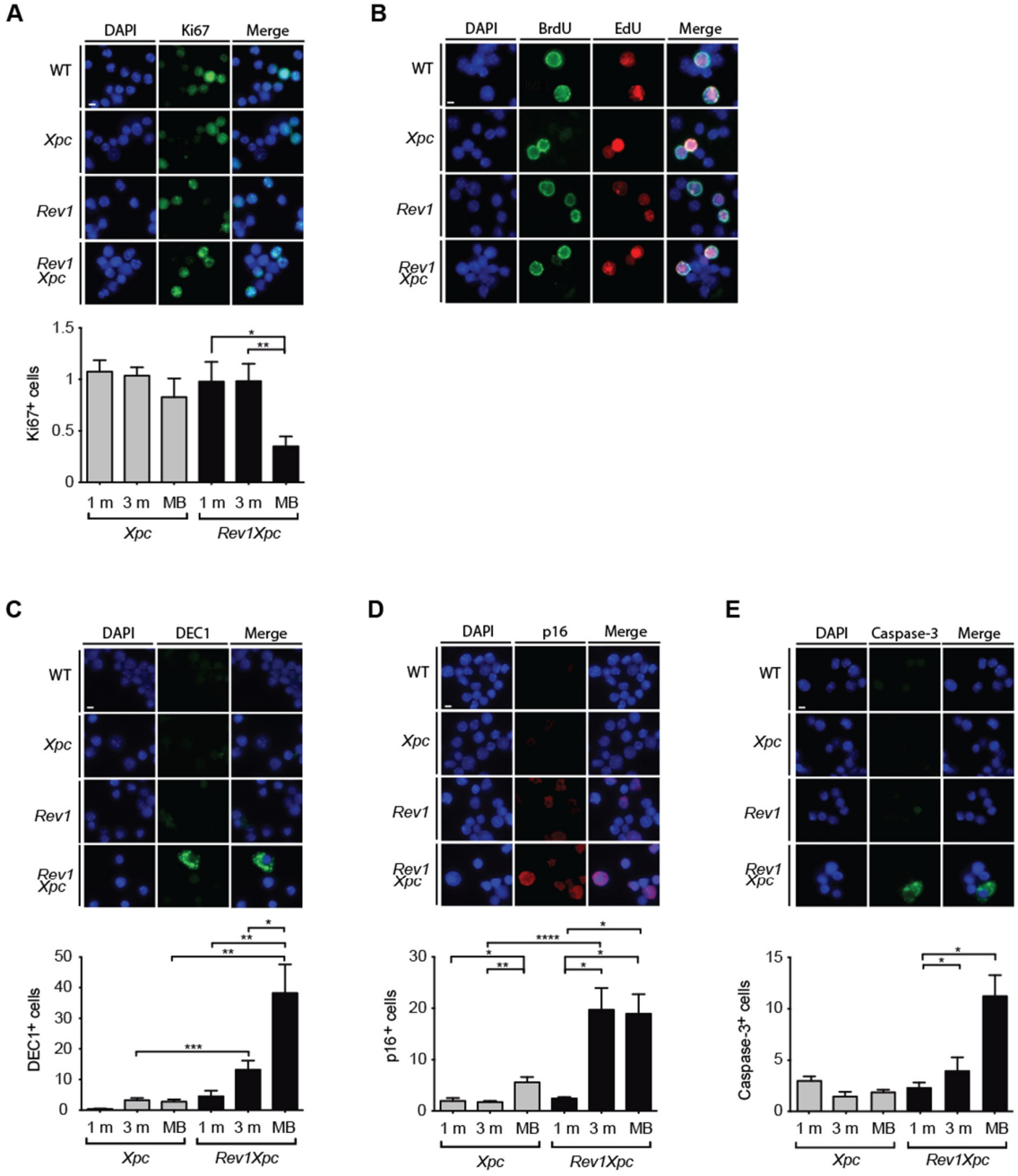

A, B. Representative staining for proliferation (Ki67; A) and replication (BrdU+EdU; B) in 3 months old bone marrow cells. Bottom panel A: quantification of Ki67 staining in *Xpc* and *Rev1Xpc* bone marrow cells at the age of 1 and 3 months, and at death (MB).

C, D, E. Representative staining for senescence (DEC-1; C and p16; D), and for apoptosis (Caspase-3; E) in 3 months old bone marrow cells. Bottom panels C, D: quantification of DEC-1, p16 and Caspase-3 staining in *Xpc* and *Rev1Xpc* bone marrow cells at the age of 1 and 3 months, and at death (MB).

SUPPLEMENTAL FIGURE 6. Progressive oxidative stress and mitochondrial dysfunction in the bone marrow of *Rev1Xpc* mice.

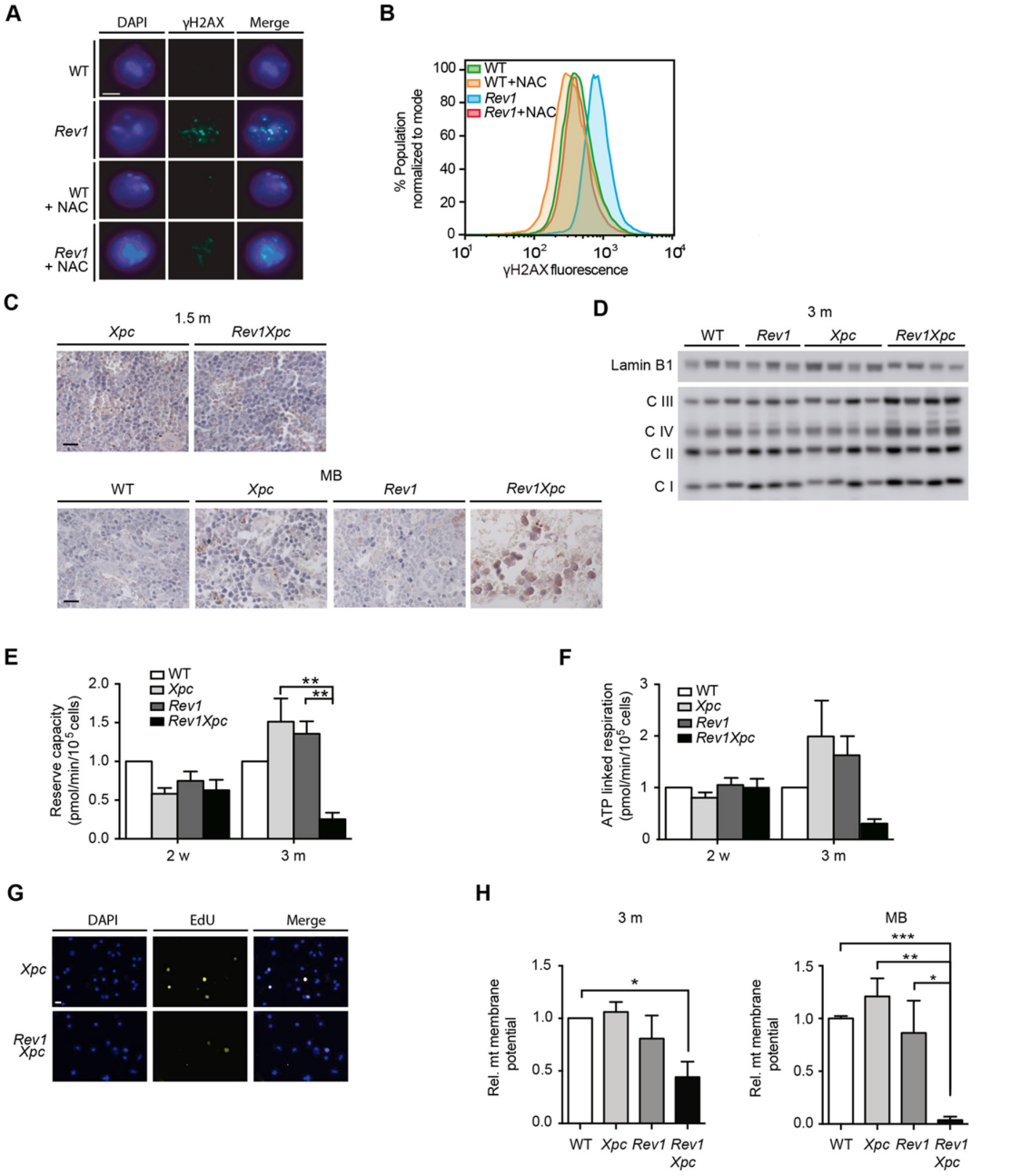

*p < 0.05. **p <0.01. Data are mean ± S.E.M.

A. Staining for the replication stress and breaks marker γH2AX in WT and *Rev1* HSC, cultured in the absence or presence of the radical scavenger N-acetylcysteine (NAC).

B. Representative analysis by bivariate cytometry of γH2AX expression in WT (n=3) and *Rev1* (n=3) HSC, cultured in the presence or absence of NAC. Horizontal axis: staining intensity, vertical axis: cell number.

C. Staining for the oxidative stress marker and DNA damaging agent 4-HNE in bone marrow. Representative pictures of n=3 per genotype. Bar: 25 μm.

D. Representative Western blot of mitochondrial complexes I-IV in bone marrow of WT (n=3), *Xpc* (n=4), *Rev1* (n=3) and *Rev1Xpc* (n=4) mice. LaminB1: internal standard.
E. Reserve mitochondrial respiratory capacity in living cells from bone marrow of WT, *Xpc*, *Rev1* and *Rev1Xpc* mice, normalized to *Xpc*. 2 w (n=6), 3 m (n=3). W: weeks.
F. ATP-linked mitochondrial respiratory capacity in living cells from bone marrow of WT, *Xpc*, *Rev1* and *Rev1Xpc* mice, normalized to *Xpc*. 2 w (n=5-6), 3 m (n=3).
G. Replication (EdU incorporation by injection 1 hour before sacrificing) in bone marrow of *Xpc* and *Rev1Xpc* mice. WT: 2 w (n=5-6), 3 m (n=3).
H. Mitochondrial membrane potentials in 3 months-old and moribund mice of all genotypes.